

3-2023

THE THREE-DIMENSIONAL VISUALIZATION OF MARS DUST STORMS BASED ON DERIVING DIGITAL ELEVATION MAPS FROM SATELLITE IMAGERY

Meirah Ali Alzeyoudi
United Arab Emirates University

Follow this and additional works at: https://scholarworks.uaeu.ac.ae/all_theses



Part of the [Physics Commons](#)

Recommended Citation

Alzeyoudi, Meirah Ali, "THE THREE-DIMENSIONAL VISUALIZATION OF MARS DUST STORMS BASED ON DERIVING DIGITAL ELEVATION MAPS FROM SATELLITE IMAGERY" (2023). *Theses*. 1055.
https://scholarworks.uaeu.ac.ae/all_theses/1055

This Thesis is brought to you for free and open access by the Electronic Theses and Dissertations at Scholarworks@UAEU. It has been accepted for inclusion in Theses by an authorized administrator of Scholarworks@UAEU. For more information, please contact mariam_aljaberi@uaeu.ac.ae.

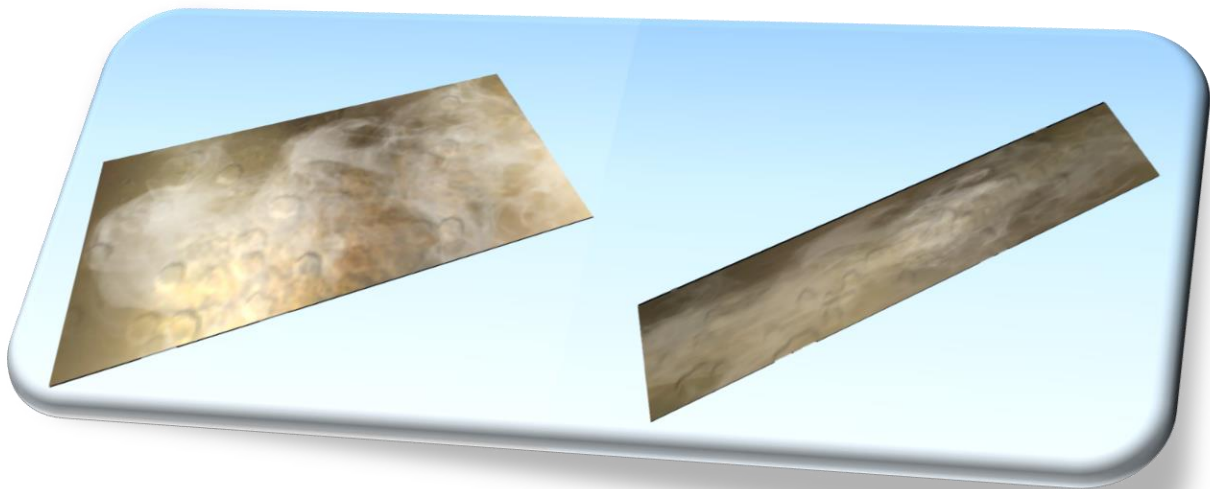
MASTER THESIS NO. 2023: 27

College of Science

Department of Physics

**THE THREE-DIMENSIONAL VISUALIZATION OF
MARS DUST STORMS BASED ON DERIVING DIGITAL
ELEVATION MAPS FROM SATELLITE IMAGERY**

Meirah Ali Alzeyoudi



March 2023

United Arab Emirates University

College of Science

Department of Physics

THE THREE-DIMENSIONAL VISUALIZATION OF MARS DUST
STORMS BASED ON DERIVING DIGITAL ELEVATION MAPS
FROM SATELLITE IMAGERY

Meirah Ali Alzeyoudi

This thesis is submitted in partial fulfilment of the requirements for the degree of Master
of Space Science

March 2023

United Arab Emirates University Master Thesis

2023: 27

Cover: A three-dimensional visualization of two local dust storms, in the left is the first local dust storm that occurred on May 20, 2020, in the Chryse Planitia Region of Mars, while on the right is the second one which occurred on 8 June 2021, on the northern side of the Utopia Planitia Region of Mars.

(Photo: By Meirah Alzeyoudi)

© 2023 Meirah Ali Alzeyoudi, Al Ain, UAE

All Rights Reserved

Print: University Print Service, UAEU 2023

Declaration of Original Work

I, Meirah Ali Alzeyoudi, the undersigned, a graduate student at the United Arab Emirates University (UAEU), and the author of this thesis “*The Three-Dimensional Visualization of Mars Dust Storms Based on Deriving Digital Elevation Maps from Satellite Imagery*”, hereby, solemnly declare that this is the original research work done by me under the supervision of Dr. Abdelgadir Abuelgasim, in the College of Humanities and Social Science at UAEU. This work has not previously formed the basis for the award of any academic degree, diploma or a similar title at this or any other university. Any materials borrowed from other sources (whether published or unpublished) and relied upon or included in my thesis have been properly cited and acknowledged in accordance with appropriate academic conventions. I further declare that there is no potential conflict of interest with respect to the research, data collection, authorship, presentation, and/or publication of this thesis.

Student's Signature:



Date: 24 -04-2023

Advisory Committee

1) Advisor: Dr. Abdelgadir Abuelgasim

Title: Associate Professor

Department of Geography and Urban Sustainability
College of Humanities & Social Science

2) Co-advisor: Dr. Claus Gebhardt

Title: Assistant Professor

College of Science and National Space Science and Technology Center

Approval of the Master Thesis

This Master Thesis is approved by the following Examining Committee Members:

- 1) Advisor (Committee Chair): Dr. Abdelgadir Abuelgasim
Title: Associate Professor
Department of Geography and Urban Sustainability
College of Humanities & Social Science

Signature  Date 22-05-2023

- 2) Member: Dr. Claus Gebhardt
Title: Assistant Professor
The National Space Science and Technology Center

Signature  Date 22-05-2023

- 3) Member (Internal Examiner): Dr. Aquib Moin
Title: Associate Professor
Department of Physics
College of Sciences

Signature  Date 22-05-2023

- 4) Member (External Examiner): Dr. Maria-Paz Zorzano
Title: Honorary Professor and Staff Researcher
Institution: CAB (Astrobiologz Center), National Institute for Aerospace
Technology INTA, Torrejon de Ardoz, Madrid, Spain

Signature  Date 22-05-2023

This Master Thesis is accepted by:

Dean of the College of Science: Professor Maamar Benkraouda

Signature Maamar Benkraouda

Date June 1, 2023

Dean of the College of Graduate Studies: Professor Ali Al-Marzouqi

Signature Ali Hassan

Date June 2, 2023

Abstract

This work focuses on generating a Three-Dimensional Visualization of Mars's local dust storms utilizing satellite images from publicly available archives. The work aimed to create a Three-Dimensional Visualization of two Local Dust storms, the first local dust storm occurred on May 20, 2020, in the Chryse Planitia Region of Mars, while the second one occurred on 8 June 2021, on the northern side of the Utopia Planitia Region of Mars. The visualization will assist in providing a better understanding of the dynamics of Dust Storms on Mars by indicating and analyzing the main features of dust storms on Mars. Also, describe the steps required to create a Three-Dimensional Visualization using several missions, tools, and software. The workflow began with the MeteoMARS tool identifying the Local Dust Storm by viewing global maps of Mars from the Mars Color Imager\ Mars Reconnaissance Orbiter Mission. Following that, observation of Local Dust Storms. Then, using The Cartography and Imaging Sciences Discipline Node of the Planetary Data System to download the images and The Integrated Software for Imagers and Spectrometers processes the images and generates the files required for calculating the main features of a Mars dust storms such as the Sun azimuth angle and the Sun incidence angle of the dust storm. Then, the calculations of the dust height from the dust storm's shadow began. Furthermore, for the visualization, a generation of 6 tables listing the Dust Storm Heights associated with each longitude and latitude. The visualization was then created using PYTHON and QGIS software. According to the findings, the first dust storm (20 May 2020) had a maximum height of 43.02 km at -28.8534 longitude and 24.6740 latitudes, while the second dust storm (8 June 2021) obtained a maximum vertical height of 47 km at 117.401 longitude and 54.892 latitudes. Moreover, the horizontal expansion for both was less than 2000 km; the first dust storm obtained around 1200 km horizontally, while the second dust storm reached around 1700 km, indicating local dust storm characteristics (local dust storms have an area of less than 1.6 million square km and under 2000 km horizontal expand).

Keywords: Three-Dimensional Visualization, Mars, Local Dust Storms, Dust, Satellite Images, Dust Storm Height.

Title and Abstract (in Arabic)

التصور ثلاثي الأبعاد للعواصف الترابية على المريخ استنادًا إلى اشتقاق خرائط الارتفاع الرقمية من صور الأقمار الصناعية

الملخص

يركز هذا العمل على إنشاء تصور ثلاثي الأبعاد للعواصف الترابية المحلية للمريخ باستخدام صور الأقمار الصناعية من الأرشفات المتاحة للجمهور. يهدف العمل إلى إنشاء تصور ثلاثي الأبعاد لعاصفتين غباريتين محليتين، حيث وقعت أول عاصفة ترابية محلية في 20 مايو 2020، في منطقة Chryse Planitia بالمريخ، بينما حدثت الثانية في 8 يونيو 2021 في منطقة Utopia Planitia في المريخ. وسيساعد هذا التصور لتوفير فهم أفضل لديناميكيات العواصف الترابية على المريخ من خلال الإشارة إلى السمات الرئيسية للعواصف الترابية على المريخ وتحليلها. وصف أيضًا الخطوات المطلوبة لإنشاء تصور ثلاثي الأبعاد باستخدام العديد من المهام والأدوات والبرامج. بدأ سير العمل باستخدام أداة MeteoMARS التي تحدد عاصفة الغبار المحلية من خلال عرض الخرائط العالمية للمريخ من مهمة المريخ Mars Color Imager \ Reconnaissance Orbiter Mission. بعد ذلك، رصد العواصف الترابية المحلية. ومن ثم، باستخدام The Cartography and Imaging Sciences Discipline Node of the Planetary Data System لتنزيل الصور، ثم يقوم برنامج Spectrometers بمعالجة الصور وإنشاء الملفات المطلوبة لحساب السمات الرئيسية للعواصف الترابية على المريخ مثل سمت الشمس الزاوية وزاوية سقوط الشمس للعاصفة الترابية. ثم بدأت حسابات ارتفاع الغبار من ظل العاصفة الترابية. علاوة على ذلك، من أجل التصور، هناك جدولين يسردان ارتفاعات الغبار المرتبطة بكل خط طول وخط عرض. تم إنشاء التصور بعد ذلك باستخدام البرامج التالية PYTHON و QGIS. وفقًا للنتائج الجداول والتصوير الثلاثي الأبعاد، بلغ أقصى ارتفاع للعاصفة الترابية الأولى (20 مايو 2020) 43.02 كم عند خط طول -28.8534 وخط عرض 24.6740، بينما حصلت العاصفة الترابية الثانية (8 يونيو 2021) على ارتفاع رأسي أقصى يبلغ 47 كم عند خط طول 117.401 وخط عرض 54.892. علاوة على ذلك، كان التمدد الأفقي لكليهما أقل من 2000 كم؛ حصلت العاصفة الترابية الأولى على حوالي 1200 كم أفقيًا، بينما وصلت العاصفة الترابية الثانية إلى حوالي 1700 كم، مما يشير إلى خصائص العاصفة الترابية المحلية (تبلغ مساحة العواصف الترابية المحلية أقل من 1.6 مليون كم مربع وتقل عن 2000 كم في التوسع الأفقي).

مفاهيم البحث الرئيسية: تصور ثلاثي الأبعاد، كوكب المريخ، عواصف الغبار المحلية، الغبار، صور الأقمار الصناعية، ارتفاع عاصفة الغبار.

Author Profile

I am Meirah Alzeyoudi, Since January 2021, I have been a student in the Master of Science in Space Science Program in the Physics department at United Arab Emirates University (UAEU) under the supervision of Dr. Abdelgadir Abuelgasim. I am also an Urban Planner at Dibba Municipality working on building a database for the uniting program at the Municipality and using AutoCAD and ArcMap for creating site plans. As well as I received my training at the National Space Science and Technology Center (NSSTC) with Dr. Claus Gebhardt from the UAE University. My training at the NSSTC was an important element for my MSc degree since it allowed me to obtain knowledge and practical experience in Space Science while meeting the master's thesis requirement. My work at the NSSTC was focused on Mars dust storms.

As part of my master's degree work, I participated in April 2023, as the first author of an Oral presentation, in the EGU conference in Vienna, Austria. The presentation was titled "*The Three-Dimensional Visualization of Mars Dust Storms Based on Deriving Digital Elevation Maps from Satellite Imagery*".

I obtained a Bachelor of Urban planning with a minor in Geographic information systems from UAEU in June 2020. During my undergraduate studies, I took part in several conferences and seminars. One of them was my presentation about the Alternate Future for Al Ain City Using GeoDesign at the ESRI Conferences in Redland, CA, USA, in February 2020.

Acknowledgments

I would like to thank my committee for their guidance, support, and assistance throughout the preparation of this thesis, especially my advisor Dr. Abdelgadir Abuelgasim and my co-advisor Dr. Claus Gebhardt.

Special acknowledgment goes to the National Space Science and Technology Center (NSSTC) for giving me the opportunity and support, including financial support through the MSc Space Science Scholarship, to continue my master's degree.

Dedication

*To my beloved parents and family
Ali Alzeyoudi, Fawzeyah Alkhzaimi*

Table of Contents

Title	i
Declaration of Original Work.....	iii
Advisory Committee.....	iv
Approval of the Master Thesis	v
Abstract.....	vii
Title and Abstract (in Arabic).....	viii
Author Profile	ix
Acknowledgments	x
Dedication.....	xi
Table of Contents.....	xii
List of Tables	xiv
List of Figures.....	xv
List of Abbreviations	xvii
Chapter 1: Introduction.....	1
1.1 Overview	1
1.2 Statement of the Problem	3
1.3 Research Objectives	4
1.4 Relevant Literature	5
1.4.1 Dust on Mars.....	5
1.4.2 Dust Activities on Mars and Earth.....	6
1.4.3 History of Dust Storms Studies on Mars	7
1.4.4 Dust storms on Mars	8
1.4.5 The Chryse Planitia Region of Mars and Dust Activities.....	10
1.4.6 The Utopia Planitia Region of Mars and Dust Activities	12
1.4.7 The Relationship Between Dust storms and Temperature.....	13
1.4.8 Effects of Dust and Dust storms	14
1.4.9 Dust Hight from the Shadow	16
1.5 Data Description.....	19
1.5.1 MARCI \MRO Mission	19
1.5.2 PDS Imaging Node of NASA	20
1.5.3 USGS	21

1.5.4 Nasa Integrated Software for Imagers and Spectrometers.....	22
1.5.5 MeteoMARS	22
1.5.6 QGIS	23
Chapter 2: Methods.....	24
2.1 Methods	24
2.1.1 Downloading MARCI\MRO image.....	24
2.1.2 Processing MARCI image	27
2.1.3 Project the Image into a Cylindrical Map Projection.....	29
2.1.4 Calculations of the Length of the Dust Storm Shadows from the Image	31
2.1.5 Calculations of the Height of the Dust Storm	34
Chapter 3: Results and Discussions.....	35
3.1 Overview of the Main Findings.....	35
3.1.1 Table with Needed Parameters for the Visualization.....	35
3.1.2 Determine the Horizontal Expand of the Local Dust Storm.....	41
3.1.3 Three-Dimensional Visualization using PYTHON.	43
Chapter 4: Conclusion	57
References.....	60
Appendix.....	65

List of Tables

Table 1: The Parameters Needed for the Incremental Dust Storm	
Height of the Local Dust Storm from 20 May 2020.	35
Table 2: The Parameters Needed for the Incremental Dust Storm	
Height of the Local Dust Storm from 8 June 2021.	37

List of Figures

Figure 1: First image of mars surface captured by Viking 1.....	1
Figure 2: Mars seasons and when Mars is closest to the sun.	9
Figure 3: A map depicts the landing sites of successful Mars missions.	11
Figure 4: A dust storm was observed in the Utopia Planitia region of Mars.	12
Figure 5: The impact of three regional dust storms on temperature.....	13
Figure 6: The damage to the Curiosity's aluminum wheel caused by Mars dust.	14
Figure 7: The last incomplete image taken by NASA's Opportunity rover.	15
Figure 8 : An image from MARCI\MRO images with a clear dust storm shadow generated from this work Chapter 2 processing a dust storm that occurred on May 20, 2020, using Nasa integrated softwires for imageries and spectrometers.	16
Figure 9: A Geologic Map of Mars created by the US Geological Survey.....	21
Figure 10: A 3D of DEM and vector data using the Qgis2threejs plugin from QGIS.....	23
Figure 11: Using the MeteoMars tool to view a dust storm (20 May 2020).	25
Figure 12: The local dust storm that occurred on 20 May 2020 using MeteoMars.	26
Figure 13: The dust storm that occurred on 8 June 2021 using MeteoMars.	26
Figure 14: MARCI instrument each band and the wavelength that responds to it, with a focus on information related to band number 4 that was used in this work.	28
Figure 15: The merged odd and even files into a cylindrical map projection.	29
Figure 16: The incidence angle file with the values in the lower right indicating the incidence angle value at a specific longitude and latitude.	30
Figure 17: The distribution of sun azimuth angles and the sun direction.	32
Figure 18: The starting point of the dust shadow at this specific shadow area.	33
Figure 19: The counting of the pixels according to the Sun Azimuth Angle and the Sun clock.	33
Figure 20: The equation used for calculating the height of the dust storm.	34
Figure 21: The horizontal expand from center of the local dust storm on 20 of May 2020.	41
Figure 22: The horizontal expand from center of the local dust storm on 6 of June 2021.	42
Figure 23: The distribution of height within the first local dust storm.	44
Figure 24: The distribution of height within the second local dust storm.....	45
Figure 25: A contour maps of both local dust storms represents the heights of dust.	46

Figure 26: A Mars DEM from MOLA\ MGS. 47

Figure 27: The map displays the DEM of the study area, as well as the
distribution of the dust Heights from the local dust storm
on May 20, 2020..... 48

Figure 28: The map displays the DEM of the study area, as well as the
distribution of the dust Heights from the local dust storm
on June 8, 2021..... 49

Figure 29: The representative raster image for 20-5-2020 local dust storm 51

Figure 30: The representative raster image for 8-6-2021 local dust storm 51

Figure 31: 20 of May 2020 local dust storm from MeteoMars MARCI\MRO
with a dust effect. 52

Figure 32: 8 of June 2021 local dust storm from MeteoMars MARCI\MRO
with a dust effect. 52

Figure 33: 3D visualization of 20 -5-2020 local dust storm..... 53

Figure 34: 3D visualization of 8 -6-2021 local dust storm..... 54

List of Abbreviations

2D	Two- Dimensional
3D	Three-Dimensional
ENVI	Environment for Visualizing Images
GDAL	Geospatial Data Abstraction Library
GDE's	Global dust storm events
GCM	General Circulation Model
HDL	High Dust Loading
ISIS	Integrated Software for Imagers and Spectrometers
LDL	Low Dust Loading
Ls	Solar Longitude (°)
MARCI	Mars Color Imager
MCD	Mars Climate Database
MDGM's	Mars Daily Global Maps
MGS	Mars Global Surveyor
MGSMs	Mars Global Climate Models
MOC	Mars Orbiter Camera
MOLA	Mars Orbiter Laser Altimeter
MRO	Mars Reconnaissance Orbiter Mission
MY	Mars Year
NASA	National Aeronautics and Space Administration
NOMAD	Nadir and Occultation for Mars Discovery
NSSTC	National Space Science and Technology Center
PDS	Planetary Data System
QGIS	Quantum Geographic Information System Software

TGO

Trace Gas Orbiter

USGS

United States Geological Survey

Chapter 1: Introduction

1.1 Overview

Since Viking landed on Mars in 1976 (Gerald A. Soffen, 1972), humanity's fascination with the red planet has grown. Important dust storm observations were obtained by the Viking Missions (Figure 1). Therefore, two planet-encircling dust storms were observed during the operations when the sky above the landers appeared dark red and the Sun was greatly dimmed. During the summer of 2001, a global dust storm blocked Mars' surface view (Strausberg, 2005).

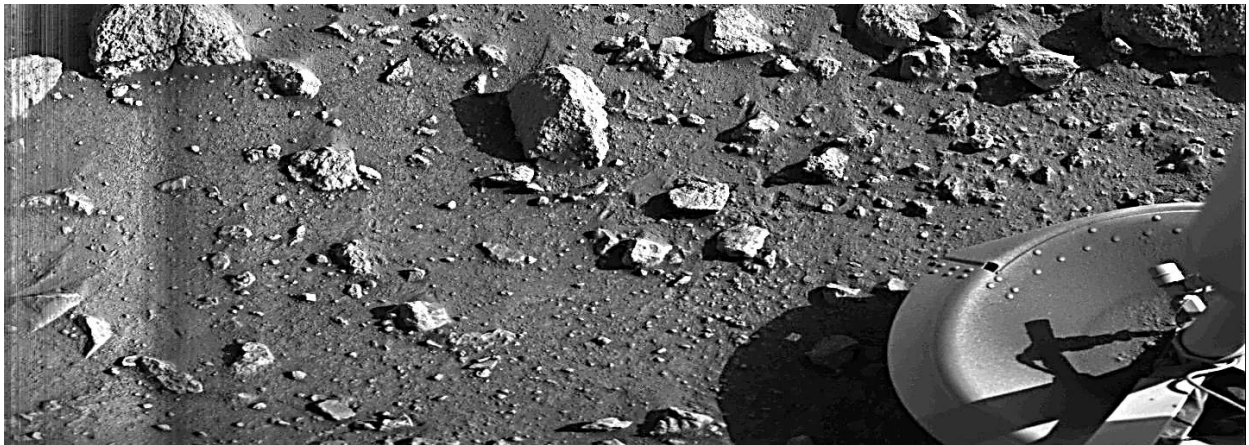


Figure 1: First image of Mars surface captured by Viking 1.

Dust is just as essential as water on Earth when it comes to Mars's weather. Martian weather may be monotonously calm for nearly half of the year due to the absence of oceans, low water vapor, and a thin atmosphere (Savijärvi, 1994). The HDL Mars dust storm occurs around perihelion, which is characterized by a relatively warm and dusty atmosphere from the southern hemisphere to the northern midlatitudes, with the solar longitude ranging from 180° to 360° (Gebhardt, 2021). However, unusual dust storms do occur during the LDL season, but local dust storms may occur at any time of the Martian year one of these local dust storms that occurred in the LDL season will be highlighted in this work.

Dust and dust storms on Mars are crucial to understanding the planet's climate and atmosphere (Yiğit, 2023). Using MARCI\MRO images, this work will demonstrate the creation of a Three-Dimensional Visualization for two local dust storms from both seasons HDL and LDL.

Through this work, observing and visualizing dust storms on Mars from satellite images can be achieved through various methods. The second chapter will outline the methods used to generate a three-dimensional visualization of a dust storm, starting with identifying the storm from an image through the naked eye. Additionally, Advanced techniques, such as comparing red and blue channel images, can be used to detect the presence of a dust storm on Mars (Cantor BA, 2001). A variety of tools, including the Meteors tool, can be used to view MARCI\MRO images. Raw images were downloaded from the NASA PDS and the images were processed using the NASA Integrated Software for Imagers and Spectrometers. This software includes a variety of functions for viewing, editing, and processing images. After selecting a dust storm, the software was utilized to edit the image. Then, using calculations, determine the dust height from the shadow projected in the image.

The third chapter of the work will include a table for each dust storm that illustrates the incremental heights of each chosen point within the storms, along with its longitude and latitude. This data will then be visualized using PYTHON and QGIS software. The first result will be a three-dimensional visualization of the height distribution of each dust storm, followed by a contour map that displays all dust heights for both storms. Both visualizations were created using PYTHON. In addition to PYTHON, QGIS software was used to create several visualizations. This chapter of the work will provide a step-by-step of creating three-dimensional visualizations based on the dust heights from the tables. Finally, the final chapter of the work will summarize the main findings and conclusions.

1.2 Statement of the Problem

Mars has always fascinated humans, but exploration has revealed some unique challenges. One of the most significant challenges explorer's faces is the notorious dust storms that can cover the planet for weeks or even months. Mars has the most dust in our solar system, which is composed of small, fine particles that are easily disturbed by the winds that constantly move across the planet's surface causing massive dust storms some can reach up to 80 km and can cause a wide range of effects to the atmosphere, temperature.

As well as dust storms have an impact on mission operations. When large-scale dust storms occur, spacecraft can enter safe modes, effectively preventing them from operating until the storm passes. Further, this could have a deleterious impact on any Mars mission, particularly if the storm lasts for weeks or months. Dust storms have even forced missions to end prematurely because the dust prevents sunlight from reaching solar panels, affecting spacecraft operations. Furthermore, local dust storms can intermission robotic rovers and other surface equipment, so understanding their behavior and characteristics is critical to the success of any future missions.

Most dust storms are only visible in 2D from satellite imagery, making it difficult to estimate the above-ground height of the dust storms by eye. As a consequence, 3D visualizations of Mars dust storms are beneficial. These visualizations can assist scientists and engineers understand the challenges they will face when exploring Mars by providing more detailed information about the shape, extent, and height of these storms.

Creating 3D visualizations of Mars dust storms is a complex task that demands advanced visualization and data processing techniques to accurately determine the dust clouds' height and shape. On the other hand, these 3D visualizations can be extremely informative, providing critical insights into the behavior of these storms and the challenges they pose for Mars exploration.

1.3 Research Objectives

The primary objective of this work is the deep study and analysis of the characteristics of the two local dust storms on Mars. This will be accomplished using satellite images from the MARCI\MRO mission and using various software and tools. Then, the characteristics and features of these storms will be identified.

Further, one of the main objectives is to extract information on above-ground-height dust from the mathematical analysis of shadows created by dust storms, and by breaking down the dust storms into a network of mapping points, this work will be able to gain a more in-depth understanding of the dust storms' behavior.

Furthermore, this work will concentrate on developing the knowledge and expertise required to generate three-dimensional visualizations of Mars dust storms. This will entail learning about the methods and requirements for creating these visualizations, as well as using them for case studies and comparisons. Documenting the characteristics of specific dust storms will also be an essential component of the work.

Overall, as dust storms more common on Mars (Battalio, 2021), a better understanding of their effects on the planet's climate and environment is critical. As a result, the ultimate purpose is to assist in understanding the behavior and characteristics of Mars dust storms through three-dimensional visualizations.

1.4 Relevant Literature

1.4.1 *Dust on Mars*

The presence of dust on Mars has a significant impact on the future of Mars missions. Dust refers to particles smaller than 20 μm in diameter with an average size of 1.5 μm , with variations from 1-2.5 μm during large dust storms. that are formed over time by the weathering of rocks (Greeley, 1991). Winds, including dust storms and dust devils, blow sand and tiny particles around, resulting in the dust.

The majority of what we know about the mineralogy of Martian dust comes from two sources: remote spectral measurements and in situ chemical measurements (Ruff, 2004) . Therefore, A description from Morris et al. (2000) shows that the material of the Martian dust is mostly “silicate material pigmented by nanophase ferric oxide particles that are associated with an unknown amount of H_2O (Morris, 2000). As a result, the dust gives Mars its warm hue, giving it the name “Red Planet.”

1.4.2 Dust Activities on Mars and Earth

Dust storms on Mars and Earth are similar in that they are both caused by wind blowing dust and other particles into the atmosphere. However, there are significant differences between them (Renno NO, 2008). Dust storms on Mars can be much larger and last much longer than those on Earth, with multiple large-scale dust storms occurring each Martian year. Dust storms on Mars can have a significant impact on the planet's climate, whereas dust storms on Earth have much less of an impact. Further, some storms cover the entire planet and reach a height of up to 80 km (Kleinböhl, 2020). On the other hand, dust storms on Earth are typically localized and on a much smaller scale. The size difference is due to the different environmental conditions of the two planets such as Mars' thinner atmosphere (Balme, 2006) Another difference between the two is the duration of the dust storms. Martian dust storms can last for weeks or even months, whereas Earth's dust storms typically last only a few hours or days. The longer duration of Martian dust storms is also due to the planet's thin atmosphere, which allows the dust particles to stay suspended in the air for longer periods (Observatory, 2022) The impact of dust storms on climate varies between the two planets. Dust storms on Mars can have a significant impact on the planet's climate by causing changes in temperature, atmospheric pressure, and the amount of sunlight that reaches the surface. Earth's dust storms, on the other hand, have a much smaller impact on the planet's climate (Observatory, 2022).

1.4.3 History of Dust Storms Studies on Mars

Regarding global dust storms on Mars observations, a few of them have been observed, beginning with telescopic observations during the 1924-1925 oppositions (Martin, 1993). Mariner 9 orbited Mars during the slow decay of one of the global dust storms; until the dust settled, the spacecraft cameras could only see the peaks of volcanoes (Strausberg, 2005).

In 1930, telescopic observations by Antoniadi suggested a link between yellow clouds and dust storms (Antoniadi, 1930). Then, After Antoniadi many space scientists were interested in studying dust and Martian dust storms.

Mars is the first planet that people want to colonize after Earth. As a result, the importance of studying the climate, atmosphere, and gravity of Mars, among other planets, has greatly increased, and many countries were attempting to assist one another in further exploring this planet. From 1965 to 1995 Mars studies have increased indicating the following. The International Mars Project coordinated the efforts of 1,074 astronomers from the United States and other nations interested in a comprehensive study of the planet Mars and established a 24-hour surveillance program of the planet during each apparition. The I.M.P. is the primary observing program for the Mars Section Association of Lunar and Planetary Observers (A.L.P.O.). The I.M.P. archives contain 26,161 observations of Mars (JD., 2001). That shows the early fascination of scientists with Mars.

1.4.4 Dust storms on Mars

The dust has a direct impact on Martian atmospheric circulation. It mostly absorbs solar energy and absorbs/emits infrared radiation, influencing the thermal structure and dynamics of the planet's atmosphere. Dust activities recorded in the Martian atmosphere ranged into types from dust devils to local, regional, and global dust storms. Furthermore, only the greatest of those storms can be seen from Earth! Those categorized dust storms can be classified as the following, a long axis of more than 2000 km dust storms are non-local dust storms, which include local\ regional dust storms (Wang, 2015). Dust storm images captured by Mars Global Surveyor (MGS) and Mars Observer Camera (MOC) that cover regions larger than 1.6 million km² and live longer than 3 Martian days were characterized as regional dust storms (Cantor, 2007). A few regional dust storms can cause global storm dust events that can cover almost all of the planet. Furthermore, large-scale (global and regional) dust storms may last for weeks or months, having a significant impact on Mars' global atmospheric structure and circulation. Previous research indicates that a large-scale dust storm is the consequence of the aggregation of numerous smaller dust storms (Wang, 2015).

Mostly, dust storms originate from the Acidalia, Utopia, Arcadia, and Hellas. The routes used to show dust storm flow reveal that dust storms are highly asymmetric between the two hemispheres. In the south, for non-global dust storms, the main routes are primarily oriented east-west, whereas, in the north, the routes are primarily north-south and zonally concentrated into meridional channels. In several impressive cases, storms originating in the northern hemisphere are observed to “flush” through Acidalia, Arcadia, and Utopia, across the equator, and then pass in the low- and mid-southern latitudes (Wang, 2015). Some regional dust storms are typically hundreds of km in extent. Moreover, they can increase by reaching a height of 30 miles (50) km and may even reach 80 km (Forget F. a., 2017).

Dust storms often occur when the lower atmosphere is heated. Figure 2 represents Mars's seasons highlighting the summer season when dust storms are most likely to occur during the season when Mars has its perihelion which is the closest point in orbit to the sun. Every year begins with a clear, highly repeatable period between $\sim L_s=0-10$ and $\sim L_s=140$ ("Low Dust Loading" -LDL- season) during which the dust opacity gradually decays globally due to almost no dust lifting. Moreover, dust storms begin to occur after $\sim L_s=140$, but not in the same pattern every year. Dust storms mainly occurred around $\sim L_s=180$ and $\sim L_s=270$. Overall, the "High Dust Loading" (HDL) season is defined as $\sim L_s=140-360$ (Forget F. F.-L.-G.-V., 2009).

Regional dust storms appear on Mars yearly, covering continent-sized regions and occurring each year and last for weeks. In addition, there are (GDE's) Global dust storm events that on average occur about once every 3-4 Mars years which is 5.5 Earth years. According to the researcher global dust storms such as those in 2018, 2007, and 2001 begins as local/regional dust storm; therefore, they are fundamentally different from smaller, regional storms in that they grow much faster and have a greater impact on the atmosphere (Kass, 2020).

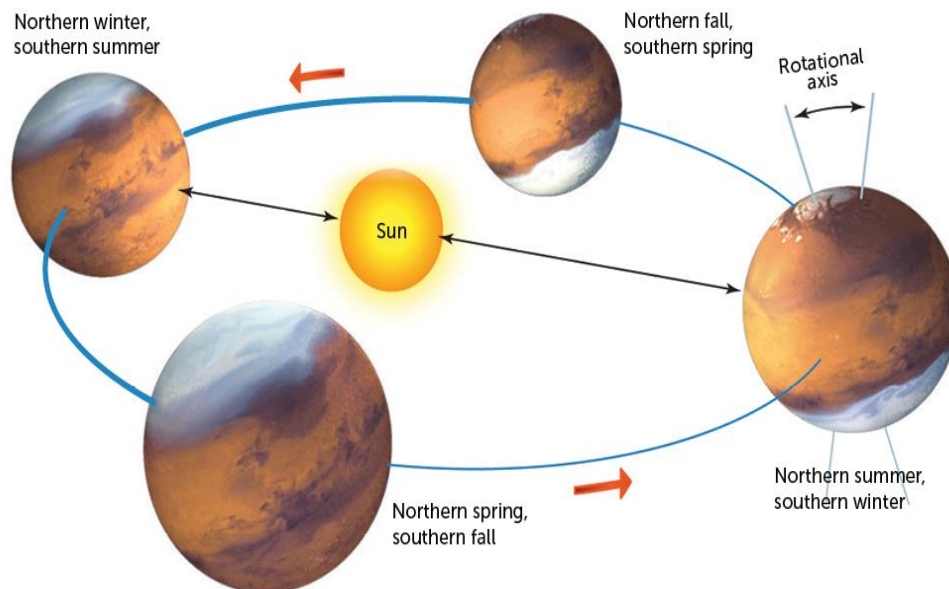


Figure 2: Mars seasons and when Mars is closest to the sun.

1.4.5 The Chryse Planitia Region of Mars and Dust Activities

Based on four Martian years of data from the Mars Orbiter Camera (MOC) and Mars Daily Global Maps (MDGMs), It has been found that 1172 dust storms were discovered around Chryse's region with a 1600 km-radius ring. Furthermore, the daily mean dust storm probability in the Chryse mission's landing region was calculated, binned by 1 of solar longitude. Also, two active dust storm periods were identified, $L_s = 177-239$ and $L_s = 288-4$, with an average daily mean dust storm probability of 9.5% and 4.1% (Li B, 2021).

The Chryse landing area was divided into square grids of 0.5 l_s and computed the average probability of dust storm occurrence in each grid, ranging from 0.19% to 2.42%, with an average of 1.22%. The chance of dust storm activity in space was generally inhomogeneous—low in the west and south but high in the east and north—and was influenced by the origin and path of dust storm sequences. According to empirical orthogonal function (EOF) analysis of storms in the Chryse region, 40.5% are northern hemisphere cap-edge storms. Finally, conclusions were reached that the ideal timing for a Mars landing mission is $L_s = 18-65$ on the Chryse Planitia, and three preferable landing places with low dust storm probability were chosen. (Li B, 2021).

1.4.5.1 Viking 1 Landing Site on the Chryse Planitia Region

Chryse Planitia is an important target region for current and future Mars landing missions because it contains several of the largest and most visible outflow channels and possible mud volcanoes. It is critical to realize that a Mars landing probe may face a dust storm situation in the Chryse Planitia during EDL season (Li B, 2021). Also, this region is considered a significant site since the Viking 1 lander landed on the western slope of Chryse Planitia, approximately near the Plains of Gold (Carr, 1980). Figure 3 shows a map of an important landing sites for successful Mars missions.

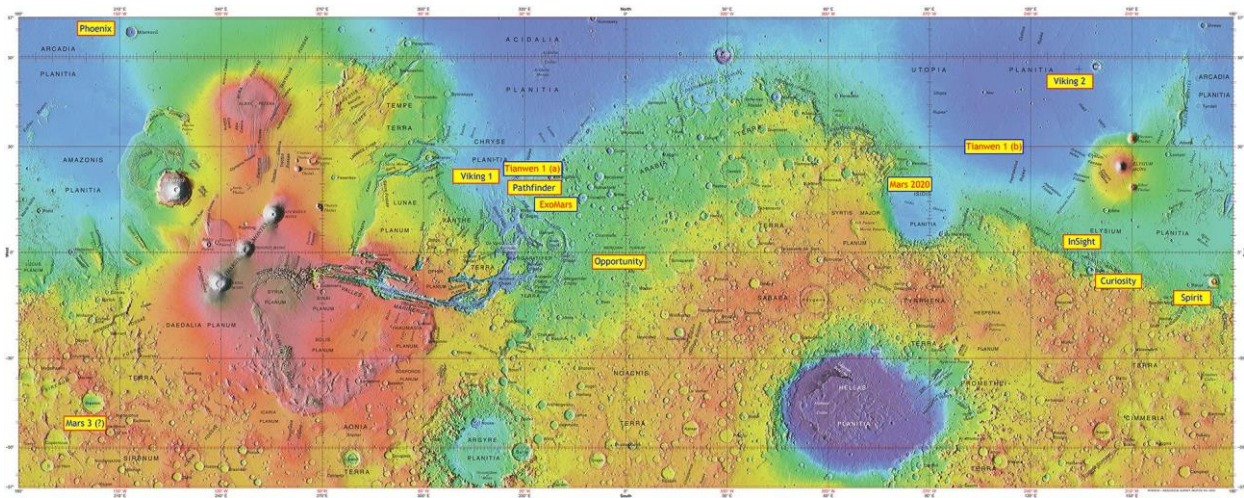


Figure 3: A map depicts the landing sites of successful Mars missions.

1.4.6 The Utopia Planitia Region of Mars and Dust Activities

Dust storms are a frequent phenomenon in Utopia Planitia, a large plain on Mars. On November 7, 2007, NASA's Mars Reconnaissance Orbiter captured images of a dust storm using the Mars Color Imager instrument. These storms are not only a visual spectacle, but they can also have significant impacts on the ongoing operations on Mars, particularly for rovers such as Curiosity and Opportunity.

NASA scientists are constantly monitoring the planet for signs of dust storms, particularly small ones that could affect ongoing missions. The image captured by the Mars Reconnaissance Orbiter, shown in Figure 4, is centered on Utopia Planitia, which is located along the north seasonal polar cap edge in late northern winter. The dust storm shown in the image was short-lived, lasting less than 24 hours (NASA, MARCI Sees a Martian Dust Storm, 2007).



Figure 4: A dust storm was observed in the Utopia Planitia region of Mars.

1.4.7 The Relationship Between Dust storms and Temperature

Dust storms have a significant impact on temperature. Therefore, the dust absorbs sunlight which raises the air temperature on Mars. In other words, dusty air warms up faster than clear air. According to (Webster, 2016), the difference between dusty and clear air can be dramatic at times, reaching up to 63F° (35C°). On this account, NASA has been operating orbiters to Mars to study its climate and temperature for decades. As stated, (Kass DM, 2016) NASA Mars orbiters have observed three types of large regional dust storms that occur at the same time every non-global-dusts-storm year in the southern hemisphere during spring and summer. Furthermore, the temperature structure during dust storms indicates an increase in temperature. In reference, Areas A, B, and C in Figure 5 as a function of latitude and time, the areas represent the times of the occurrence of the three regional dust storms, obviously observed by the Temperature Indicator that the colors at these times correspond to higher altitude temperatures.

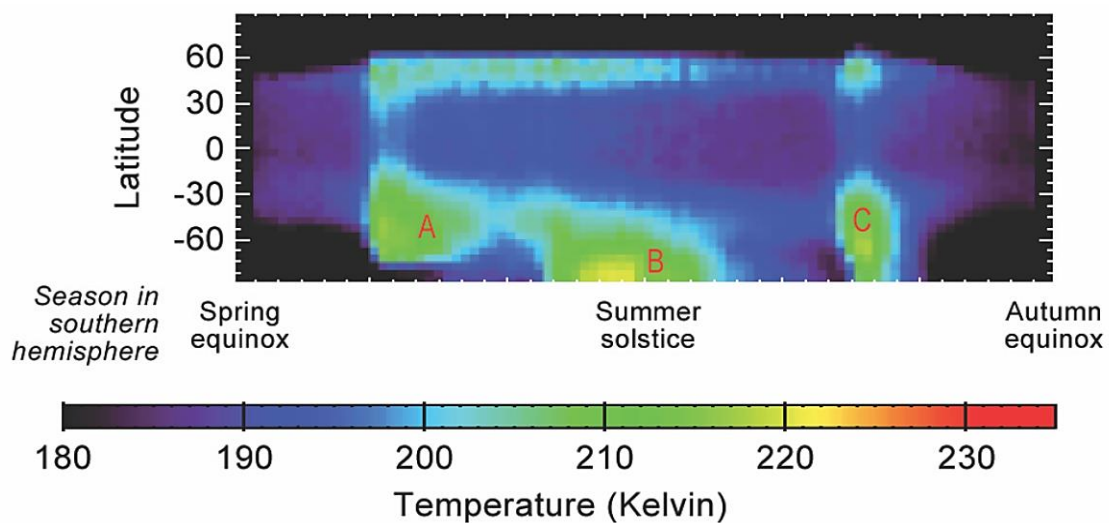


Figure 5: The impact of three regional dust storms on temperature.

1.4.8 *Effects of Dust and Dust storms*

Airborne and surface dust can influence the yearly CO₂ polar caps' formation and regression by changing the polar heat balance. Airborne dust affects the radiation balance and dynamics of the atmosphere, while surface dust affects the heat transfer performance of the surface (Kahre MA, 2010).

Further, airborne dust in Mars' atmosphere changes the energy distribution within the system because it absorbs solar energy and emits infrared radiation. Because the radiative balance of the atmosphere has such a powerful impact on atmospheric circulation, changing the amount of airborne dust causes changes in atmospheric dynamics (Kahre MA, 2010).

Dust storms could widely affect Mars missions and spacecraft. According to (Ferguson, 1999), the dust particles on Mars are very small and slightly electrostatic, which means they attach to the surfaces they come into contact with. Figure 6 indicates the damage done to the Curiosity aluminum wheel by dust. Because Martian dust particles are highly tenacious, they may stick to the gears and pose a challenge to the mechanical parts. That is why engineers must consider the properties of Martian dust particles while designing rovers for Mars. Because the dust particles stick to the solar panels, the amount of sunlight that reaches them is reduced, and less sunlight equals less energy.



Figure 6: The damage to the Curiosity's aluminum wheel caused by Mars dust.

Additionally, global dust storms can potentially cause difficulty by releasing a massive amount of dust into the Martian atmosphere, decreasing the amount of sunlight reaching the spacecraft's solar panels even more (Zubrin, 2008). To address this issue, certain spacecraft near dust storms must temporarily suspend operations until the dust storm stops, or the spacecraft at the save mode of solar power due to the reduced amount of sunlight during the dust storm (Martínez, 2017).

1.4.8.1 A Mission Ended by A Dust Storm

In January 2022, a dust storm twice the size of the United States forced NASA's Mars missions, including the Insight lander, the Ingenuity Mars Helicopter, the Mars Reconnaissance Orbiter, MAVEN, and Odyssey, to stop operations until the storm passed (NASA/JPL-Caltech, 2022). In 2018, a global dust storm also ended the agency's Opportunity rover mission because the solar panels aren't getting enough sunlight to charge the batteries, sending its last image on June 10, 2018 (Figure 7) (Cooper, 2022). Then, the rover shut down ending a 14-year run (Wall, These Are the Last Photos NASA's Opportunity Rover Took on Mars, 2019).

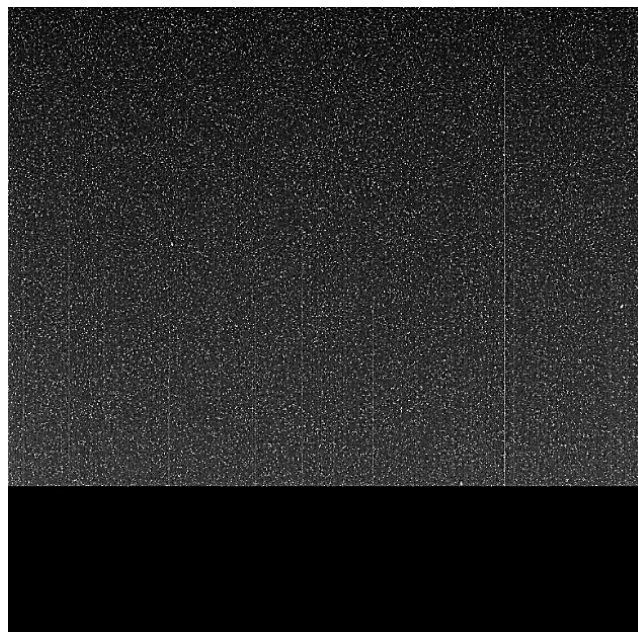


Figure 7: The last incomplete image taken by NASA's Opportunity rover.

1.4.9 Dust Hight from the Shadow

The method of determining dust storm height by analyzing the length of the dust storm's shadow is not new. Further, estimating height from shadows started with the earliest Mars missions, such as Mariner 9 (Briggs, 1974).

Dr. Iñaki Ordóñez's research investigated a local dust storm on Mars in March 2017. One of the used methods in this work was the determination of dust height using shadows cast by the dust by analyzing the length and the direction of the shadows projected by the dust storm, which can provide essential insights into the dynamics and behavior of Martian dust storms (Iñaki Ordóñez-Etxeberria, 2019). Therefore, in this work, Dr. Iñaki Ordóñez's research on this topic has made significant contributions to the understanding of dust storm behavior on Mars. As a result, his study's approach and methodology served as a valuable guide for my work (Iñaki Ordóñez-Etxeberria, 2019).

Consider a dust storm image that displays a shadow with a resolution of 1 km by 1 km (Figure 8). Each pixel of the shadow can then be counted as each pixel equals 1 km in length. By using this information, the height of the dust can be calculated through a simple mathematical formula that considers the shadow length, the sun incidence angle, and the sun azimuth angle for each pixel.



Figure 8 :An image from MARCI\MRO images with a clear dust storm shadow generated from this work Chapter 2 processing a dust storm that occurred on May 20, 2020, using Nasa integrated softwares for imageries and spectrometers.

This method has been used to estimate the height of dust in various dust storms on Mars. By determining the height of dust, scientists can better understand the behavior and impact of dust storms on the planet. For example, dust storms can affect the planet's climate and the ability of rovers and other equipment to operate on the surface (Iñaki Ordonez-Etxeberria, 2019).

It should be noted that this method of determining Dust Storm Height may not always be accurate, as the presence of clouds or other atmospheric conditions can interfere with the calculations. In addition, the resolution of the image can also affect the accuracy of the calculations. Therefore, it is important to consider multiple factors when interpreting dust storm images and estimating the height of dust.

Furthermore, to better understand dust storms, scientists use MGCMs, which are computer models that simulate the Martian atmosphere and climate, and the Mars Climate Database (MCD) which is a database of meteorological fields derived from General Circulation Model (GCM) numerical simulations of the Martian atmosphere and validated using available observational data. In the work by Ordonez-Etxeberria in 2020, the authors used a method to measure the height of dust storms on Mars. After that, they compared the results with MGCMs, they also compared their measurements with the MCD to validate their method (Iñaki Ordonez-Etxeberria, 2019).

In another study about cellular patterns and dry convection in textured dust storms at the edge of Mars's North Polar Cap, the authors also used this method and compared their results with the MCD. The MCD data can help to better understand dust storms. Therefore, their findings suggest that these dust storms can create complex cellular patterns that affect the transport of dust and heat and that these patterns can be explained by dry convection (Sánchez-Lavega, 2022).

Overall, these studies emphasize the importance of understanding the impact of dust storms on the Martian climate and spacecraft, as well as the role of MGCMs and the MCD in better understanding these phenomena.

1.4.9.1 Estimating Dust Top Heights during Mars Dust Storms using TGO/NOMAD

Researchers estimated the height of the dust top on Mars using data from the NOMAD spectrometer aboard the European Space Agency's Trace Gas Orbiter (TGO) mission. NOMAD can measure the spectral properties of sunlight at various wavelengths, allowing researchers to examine the brightness of the halo created by scattered sunlight during dust storms. Therefore, they analyze dust storms and notice that a regional dust storm got started around 7 of January and reached heights of up to 50 km (Aoki, 2019).

Further, the researchers were able to estimate the size and composition of the dust particles in the atmosphere by analyzing the spectrum of the scattered light, which allowed them to estimate the height of the dust top. This method is useful for studying dust storms on Mars because it allows researchers to gain insights into the dynamics of these storms. Furthermore, these instruments provide a wealth of data on the Martian atmosphere, which can assist researchers in learning more about the processes that cause dust storms on the planet. Researchers can continue to learn more about the Red Planet and its complex weather patterns by studying the Martian atmosphere with instruments like those on the TGO mission (Aoki, 2019).

1.5 Data Description

This work focuses on existing dust storm data, mainly from MARCI/MRO images to produce a Three-Dimensional Visualization of one of the largest local Martian dust storms.

The following have been used as a main requirement to accomplish this work:

1.5.1 MARCI\MRO Mission

The Mars Reconnaissance Orbiter, or MRO, launched on August 12, 2005, and has been researching the Red Planet's atmosphere and topography since March 10, 2006. The MRO orbiter is still operational today (Zurek, 2007).

Throughout each orbit around Mars, the Mars Color Imager MARCI captures images at seven different wavelengths, including five centered in visible-light wavelengths and two in ultraviolet wavelengths (Clancy, 2006). In a single day, MRO completes 12 to 13 orbits of Mars. MARCI images are intended to have spatial resolutions of approximately about 1-10 km per pixel range (Clancy, 2006). Those images are about 1000 pixels wide and can be many thousands of pixels long, depending on the objective of the image. By collecting this data every day for multiple Martian years, this number of images allows scientists to record each meteorological event on Mars providing a record of winter, spring, summer, and fall in both Martian hemispheres.

The MARCI\MRO science goals are to observe Martian atmospheric processes both synoptically and globally. Also, studying in detail the interaction of the Martian atmosphere and Mars's surface at various scales in both space and time. In addition, to examine surface features characteristic of the evolution of the Martian climate across time (Bell III, 2009).

1.5.2 PDS Imaging Node of NASA

The Cartography and Imaging Sciences Discipline Node of the Planetary Data System is a long-term archive of digital data that includes all the NASA planetary missions (PDS, 2023). NASA's planetary science community is using several functions from PDS. Particularly, ancillary data, advanced data explorations, search tools, and cartographic and technical expertise are required to develop and fully utilize a vast collection of digital planetary images among many terrestrial planetary bodies, including icy satellites (PDS, 2023).

Furthermore, some functions were added to improve the image processing experience. For instance, orbital and landed camera instrument development and data processing, data engineering, and informatics, planetary remote sensing at UV to RADAR wavelengths, and cartographic and geospatial data analysis and product development.

1.5.3 USGS

The US Geological Survey provides knowledge on natural hazards that threaten lives and livelihoods, the water, energy, minerals, and many other natural resources on which we depend. Furthermore, the health of our ecosystems and environment, and the effects of climate and land use change are considered (USGS, 2023). The researchers at the USGS create innovative methods and technologies to provide timely, relevant, and helpful information on the Earth and beyond and its processes.

The USGS Astrogeology Science Center has been active in Mars research, geology, cartography, and mission support. As well, the data provided morphologic, topographic, spectral, thermophysical, radar sounding, and other observations for integration, analysis, and interpretation in support of geologic mapping (Figure 9).

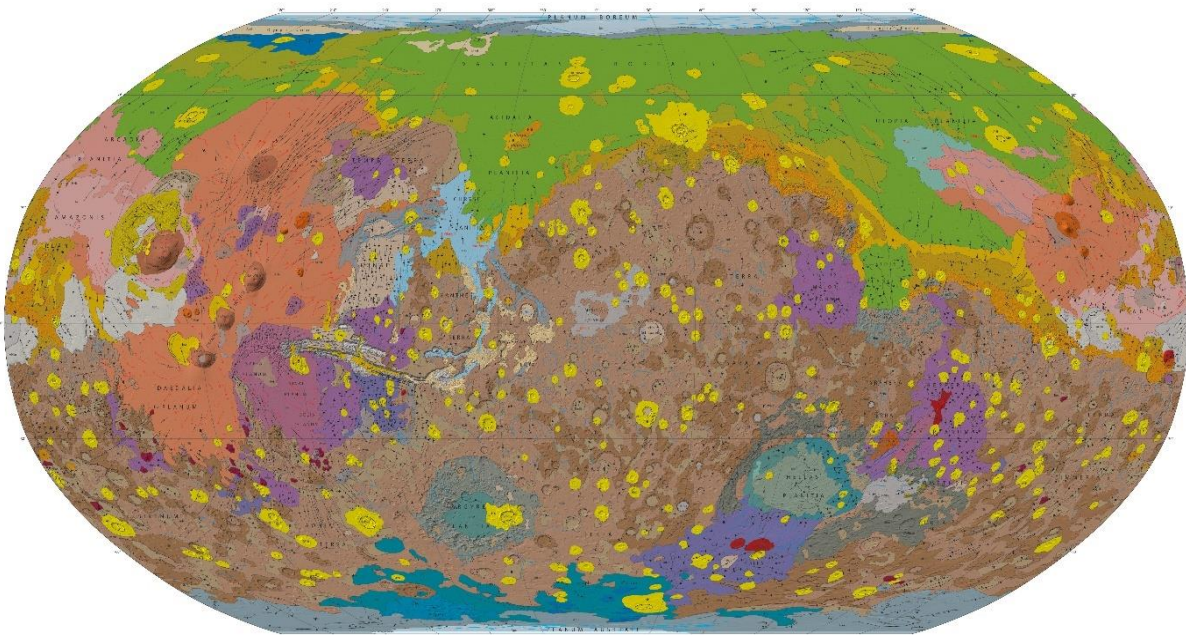


Figure 9: A Geologic Map of Mars created by the US Geological Survey.

1.5.4 Nasa Integrated Software for Imagers and Spectrometers

The USGS produced the Integrated Software for Imagers and Spectrometers (ISIS) as a free, specialized digital image processing software package. The software can place various forms of data in the correct cartographic location allowing disparate data to be co-analyzed. Also, it provides the primary image processing applications such as contrast, stretch, image algebra, filters, and statistical analysis. As well, the ISIS software analyzes both two-dimensional images and three-dimensional cubes produced by imaging spectrometers. Furthermore, it creates USGS topographic maps of extraterrestrial landing locations (ISIS, 2023). Also, it can handle data from NASA and international spacecraft missions such as Lunar Orbit, Apollo, Mars Global Surveyor, Cassini, Mars Odyssey, Mars Reconnaissance Orbiter, and many more. This work was mainly with MARCI\MRO data. Therefore, ISIS software has been chosen to process the images through this work.

1.5.5 MeteoMARS

MeteoMars is a tool that displays combined processed images to study metrology on Mars. The utility is promoted by Pamplona Planetarium, The Planetary Science Group of the University of the Basque Country, and Eng. Txus Ordorika features an adaptation of the interface developed by the project Maptoglop. This utility can process and display available PDS archives. It also shows images from MARCI\MRO. In this tool, the MARCI\MRO images are composed of a maximum of 13 images that are merged to generate a daily global map. ISIS software is used to process and merge these images (Meteo Mars, 2023).

1.5.6 QGIS

QGIS is an open-source geographic information system. The software offers a wealth of GIS functions such as viewing data, exploring data, generating, modifying, managing, and exporting data. Furthermore, the program can analyze spatial data from geographic databases. Also, it is possible to publish work that was created using the software. (QGIS, 2023).

1.5.6.1 Qgis2threejs plugin

Qgis2threejs is a powerful QGIS plugin that allows for the display of Digital Elevation Models (DEM) and vector data in 3D. With its user-friendly interface, users can easily create a variety of 3D objects and generate files for online publication. The plugin enables users to create interactive 3D visualizations that provide a unique perspective on geographic data, allowing for a better understanding and analysis of complex terrain and landscapes (QGIS, 2022).

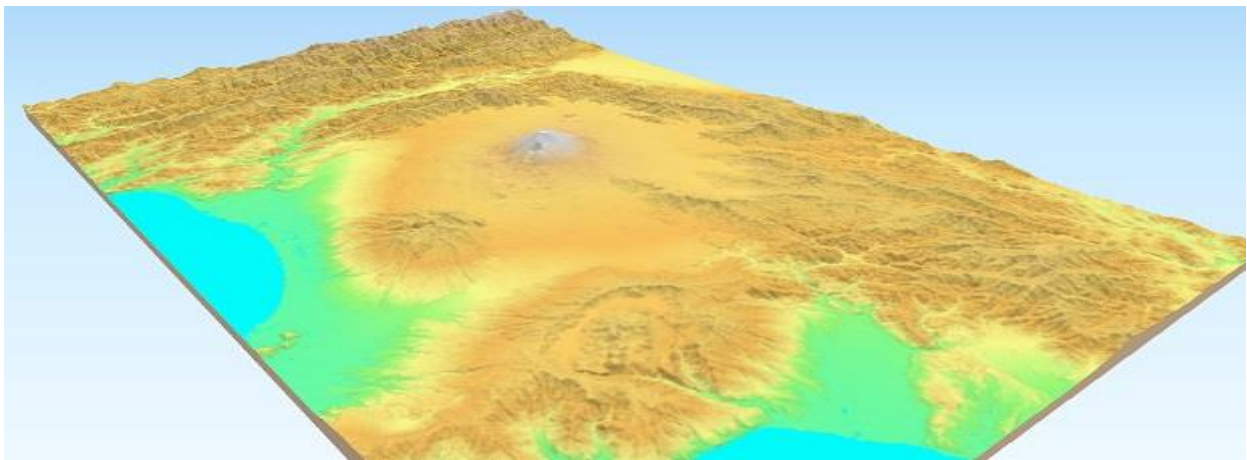


Figure 10: A 3D of DEM and vector data using the Qgis2threejs plugin from QGIS.

Chapter 2: Methods

2.1 Methods

This chapter mainly will demonstrate the methods and techniques used on the first local dust storm, which occurred on May 20, 2020. Furthermore, the methods and techniques outlined in this chapter have been applied to one additional dust storm: June 8, 2021, local dust storm (The second dust storm). Furthermore, the following chapter (chapter 3) will highlight the generation of a detailed table for each of the two dust storms, including the essential parameters for producing the Three-Dimensional visualizations.

2.1.1 Downloading MARCI\MRO image

The downloading procedure will start with the MeteoMars tool viewing MARCI\MRO images and searching for a potential dust storm. Then, the PDS will be used to download raw images of the selected dust storm.

2.1.1.1 Review the Metadata for MARCI Images

To begin, recognize the software, programs, and tools that can be used to view, edit, and visualize MARCI\MRO images. Also, the understanding of the periods and the seasons with the most dust activities (Instrument Description MARCI\MRO, 2005). Knowing that most dust activities occur from 180 to 360 ls mostly during the summer season on Mars and as I mentioned before that the High Dust Loading (HDL) season is defined as 140-360 ls. Therefore, the selection of the HDL season was done by converting the earth date to the Mars date and then highlighting the months that have a solar longitude between 140-360 ls. Then, I went through the MARCI\MRO images according to the months within the HDL season. The first dust storm occurred on May 20, 2020, during the HDL season. However, a second dust storm occurred in the LDL season on June 8, 2021. I chose this dust storm to highlight the unusual dust activity in the LDL season.

2.1.1.2 View MARCI Images

Then, after searching for suitable tools to view MARCI\MRO images, the next step was to view MARCI\MRO images and search for dust storms using the MeteoMars tool, USGS MARCI weather reports, and MDGM's (Figure 11).

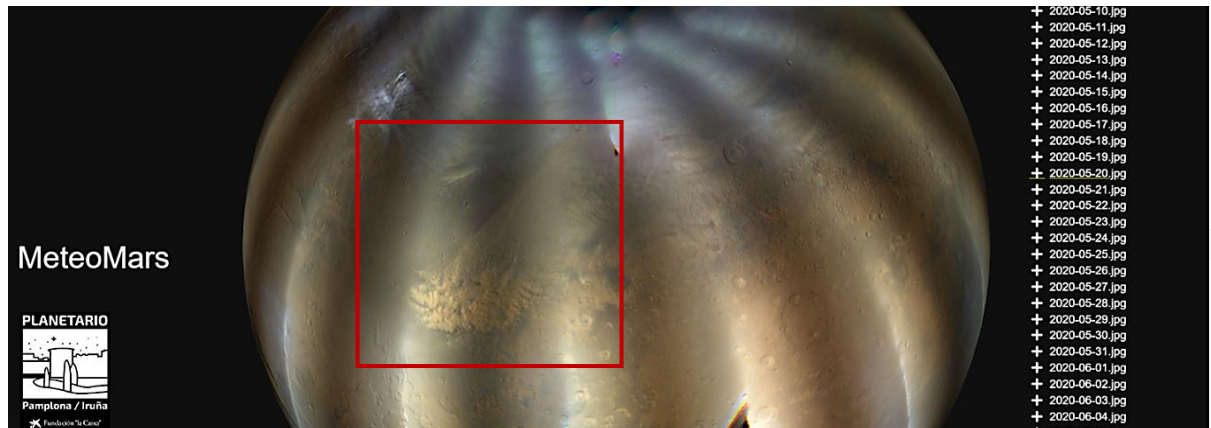


Figure 11: Using the MeteoMars tool to view a dust storm (20 May 2020).

The concentration was mostly on images from the High Dust Loading (HDL) season from 2020 to 2021 since I used the MeteoMars tool to view MARCI\MRO images, the tool has just access to MARCI\MRO images just from 2019 to 2021. Therefore, the emphasis mainly was on the year 2020, the majority of dust activities occurred in 2020 from May to December. After looking through the images, I recognized several dust storm images and decided to work on a local dust storm that occurred on May 20, 2020, in the Chryse Planitia Region at the boundary of the Arabia Terra of Mars (Figure 12). (N06 064762 2046 MA 00N018W.IMG). Then, I started taking a general look through the LDL season to determine whether any dust storms would appear during that season, and I observed my second dust storm which occurred on June 8, 2021(Figure 13).

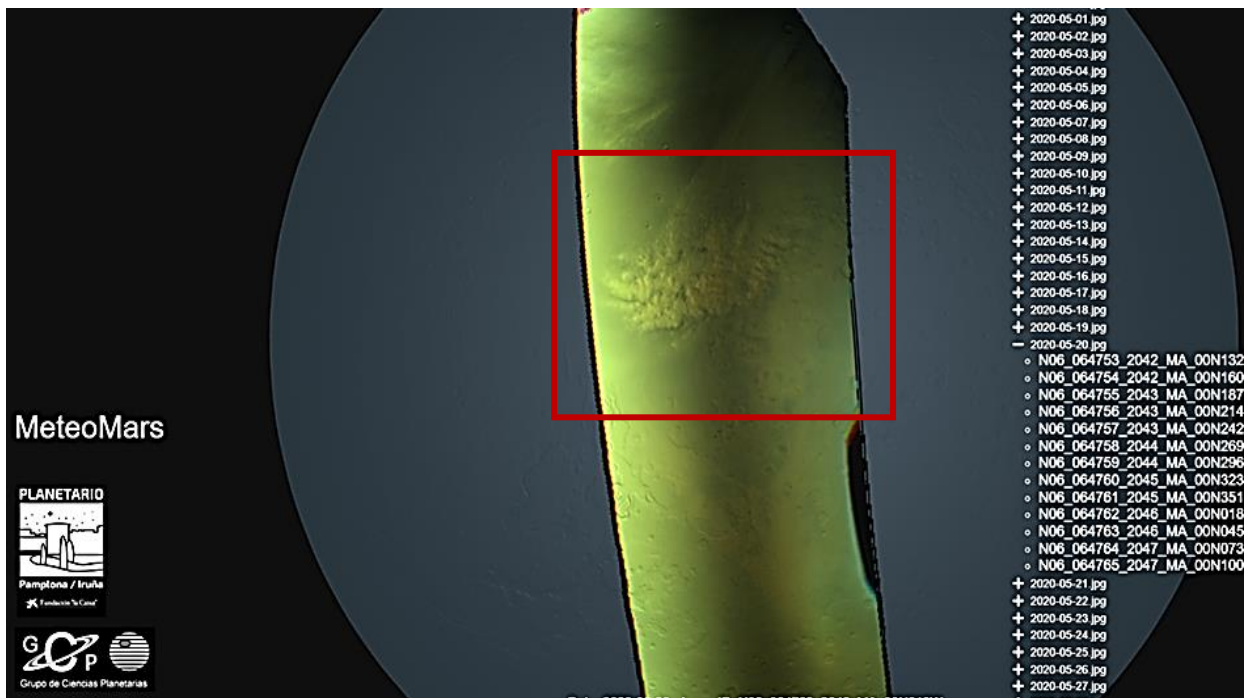


Figure 12: The local dust storm that occurred on 20 May 2020 using MeteoMars.



Figure 13: The dust storm that occurred on 8 June 2021 using MeteoMars.

2.1.1.3 Downloading MARCI Image using PDS

The downloading process from the PDS was done using the NSSTC Planetary Science Group Linux Server.

First, I looked at the DATA VOLUME INDEX section of the PDS website. After that, I chose the Mars Reconnaissance Orbiter (MRO) mission section. Following that, I went through the MARCI EDRs folder, which contains a list of folders organized by the dates on which the MARCI\MRO images were captured. Following that, I selected the Release 55 folder, which contains MARCI\MRO images from March to May 2020, the same period as the selected first dust storm. Then, while going through the files, I observed the dust storm image from May 20, 2020, under file 1203. Specifically, under (N06_064762_2046_MA_00N018W.IMG) the MARCI level 0 image. Note: In the MeteoMars tool, the specific file name appeared below the image.

2.1.2 Processing MARCI image

The NASA Integrated Software for Imagers and Spectrometers (ISIS, 2023) was used to process the MARCI\MRO image. To work with the software, the NASA Integrated Software for Imagers and Spectrometers was downloaded to the NSSTC Planetary Science Group Linux Server. Then, the following procedures have been done:

2.1.2.1 Convert the Image Format

Starting with using the MARCI2ISIS command to convert the image format to cub format. This command takes the local dust storm image captured by the MRCI\MRO and produces an Isis cube file containing all the image data. Therefore, it's important to understand that the NASA Integrated Software for Imagers and Spectrometers mostly works with cub files. The output files will generate two files, even and odd, and each will be processed independently.

2.1.2.2 Edit the Image Using Multiple Commands

Then, the application of the SPICEINIT command for both even and odd files in order to discern the SPICE kernels is required. SPICE kernels are made up of navigation and other ancillary information that provide the planetary science and engineering communities with accurate observation geometry (PDS, n.d.). After applying the SPICEINIT command, the command MARCICAL was applied for both files to do a calibration. The program basically corrects each framelet based on the band's filter number. Then, use the command EXPLODE to have each band within the image in a separate file, the focus was on red band images because using this band the dust storms images appear lighter than the rest of the image and their shadow appears darker (Shaheen F, 2022).

The band (band0004) has been chosen as the red band as known from the MARCI\MRO documentation (Instrument Description MARCI\MRO, 2005) . Knowing that from MARCI\MRO image bands categorization (Figure 14).

Band	λ_{eff}^b (nm)	πF^c (W/m ² /μm)	R [(DN/msec)/(W/m ² /μm/sr)]
		<i>VIS</i>	
1	437 ± 32	1798.4	0.806 ± 0.024
2	546 ± 40	1875.7	1.124 ± 0.009
3	604 ± 31	1742.7	0.751 ± 0.005
4	653 ± 42	1580.7	0.882 ± 0.006
5	718 ± 50	1360.3	0.777 ± 0.007
		<i>UV^d</i>	
6	258 ± 30	132.08	1.15 × 10 ⁻² ± 0.03 × 10 ⁻²
7	320 ± 24	755.64	2.50 × 10 ⁻² ± 0.04 × 10 ⁻²

4	653 ± 42	1580.7	0.882 ± 0.006
---	----------	--------	---------------

Figure 14: MARCI instrument each band and the wavelength that responds to it, with a focus on information related to band number 4 that was used in this work.

Then, the use of the PHOTOMET command performs a photometric correction on both the even and odd images of the red band pixels, adjusting the brightness and contrast so that the resulting image shows the shadows clearly.

2.1.3 Project the Image into a Cylindrical Map Projection

Then, using the command CAM2MAP, the image was projected to view the selected dust storms image. Therefore, a Simple cylindrical map projection was used because it was easy to recognize the local dust storm using it.

Then, knowing that the spatial resolution of the MARCI images ranges from 1 to 10 km per pixel. Therefore, to avoid losing any data, I rescaled the pixel resolution to 1 km, the maximum possible resolution. That resolution will be needed later for shadow calculations. Furthermore, the AUTOMOS command is used to merge odd and even files to produce the file shown below in Figure 15.

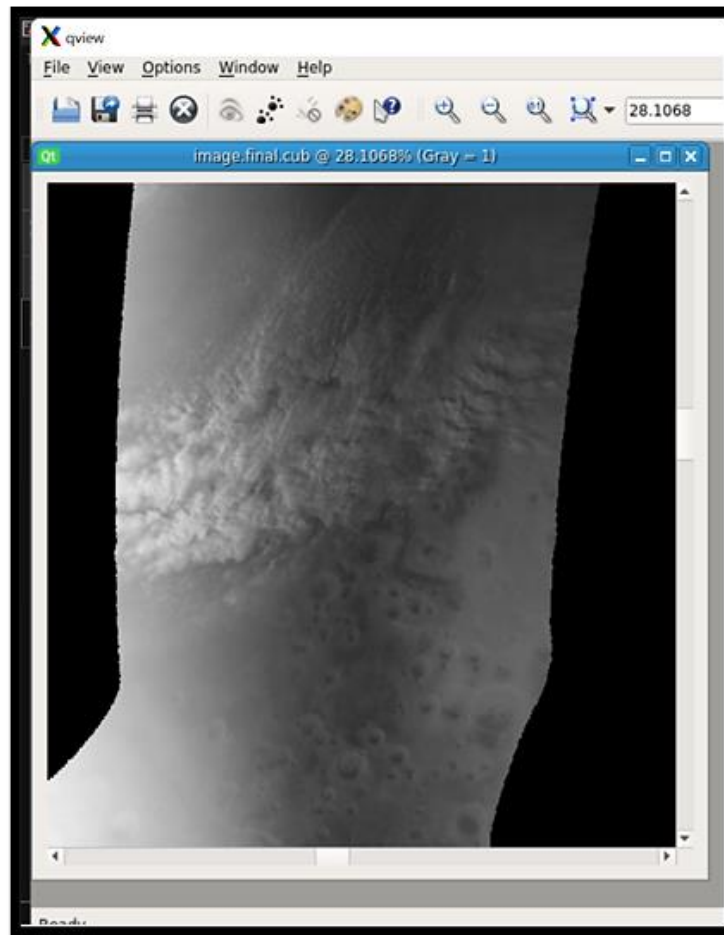


Figure 15: The merged odd and even files into a cylindrical map projection.

2.1.3.1 Production of the Needed Parameters the Sun Incidence Angle and Sun Azimuth Angle

After that, I needed the Sun incidence angle and Sun azimuth angle to calculate the dust storm's shadow length and dust heights. Therefore, the PHOCUBE command from ISIS is used to generate the needed parameters. As a consequence, in this work, this command generated two files, one for each parameter: the Sun azimuth angle for calculating shadow length and the Sun incidence angle for determining local dust storm dust heights. Note: each pixel in the produced image represents a value of the parameter (Figure 16).

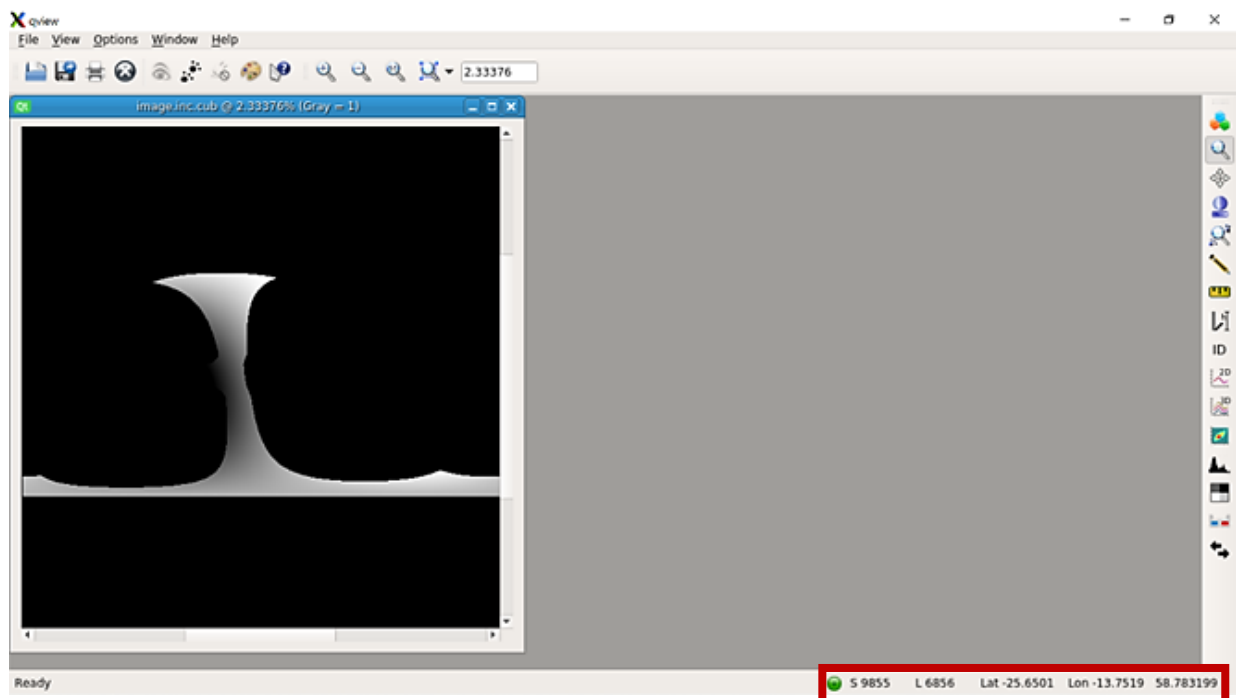


Figure 16: The incidence angle file with the values in the lower right indicating the incidence angle value at a specific longitude and latitude.

2.1.4 Calculations of the Length of the Dust Storm Shadows from the Image

The next step is to calculate the length of the dust storm's shadows in the image to determine its height. The image resolution is one km by one km, as previously discussed in Section 2.1.3, which means that each pixel in the image represents one km. However, determining the direction in which the shadow length should be measured is essential. This is where the sun's azimuth angle comes into play, as discussed in Section 2.1.3.1.

To determine the direction of the sun at each pixel, the exact point in the image file where the shadow begins is chosen. Then, in the sun-azimuth angle file, the same point is selected to indicate the angle at that time. Lastly, the sun-azimuth angle is converted into the Sun direction, and the shadow pixels are counted accordingly.

By following this procedure, we can accurately calculate the length of the shadows within the dust storm image, which will assist us in determining the height of the dust storm.

In Figure 18, if the sun azimuth angle at a specific point within the dust storm was approximately 150° (where the shadow begins in that area), the direction of the sun at that point can be determined utilizing the Sun Azimuth angles distribution in Figure 17 and the reference line in Figure 19. In Figure 17, the reference line will be calculated in the same direction as 150° . With this information, the length of the shadow can be calculated by using each pixel in the same direction as 1 km. Finally, the total shadow length around the shadow's starting point can be calculated by counting all the pixels in the same direction.

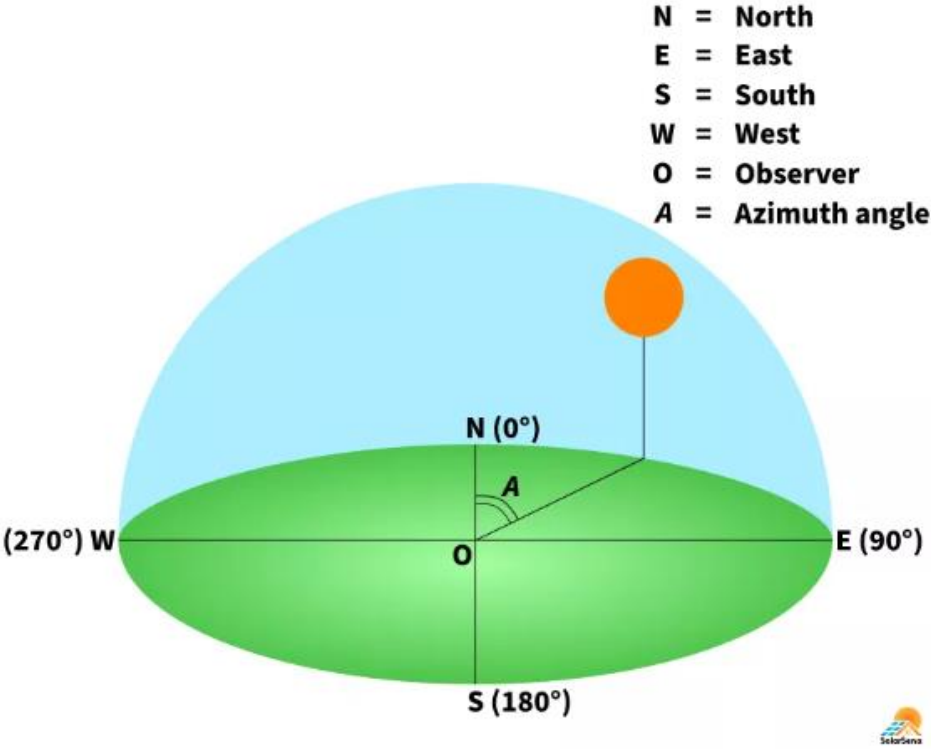


Figure 17: The distribution of sun azimuth angles and the sun direction.

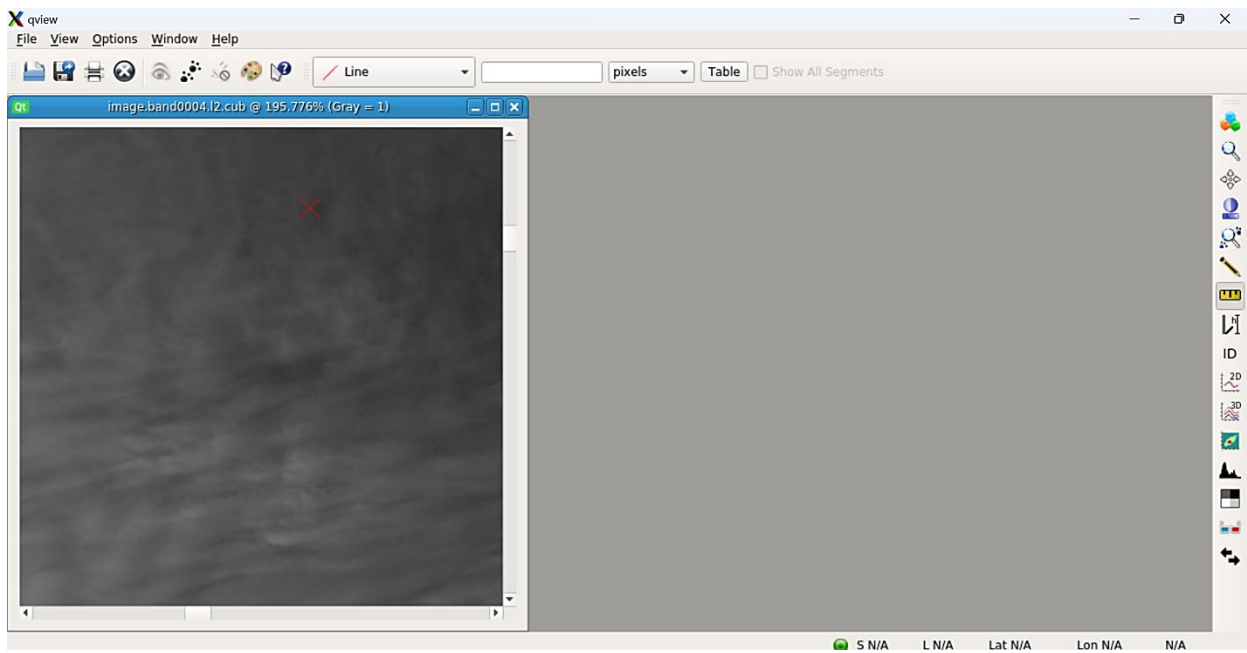


Figure 18: The starting point of the dust shadow at this specific shadow area.

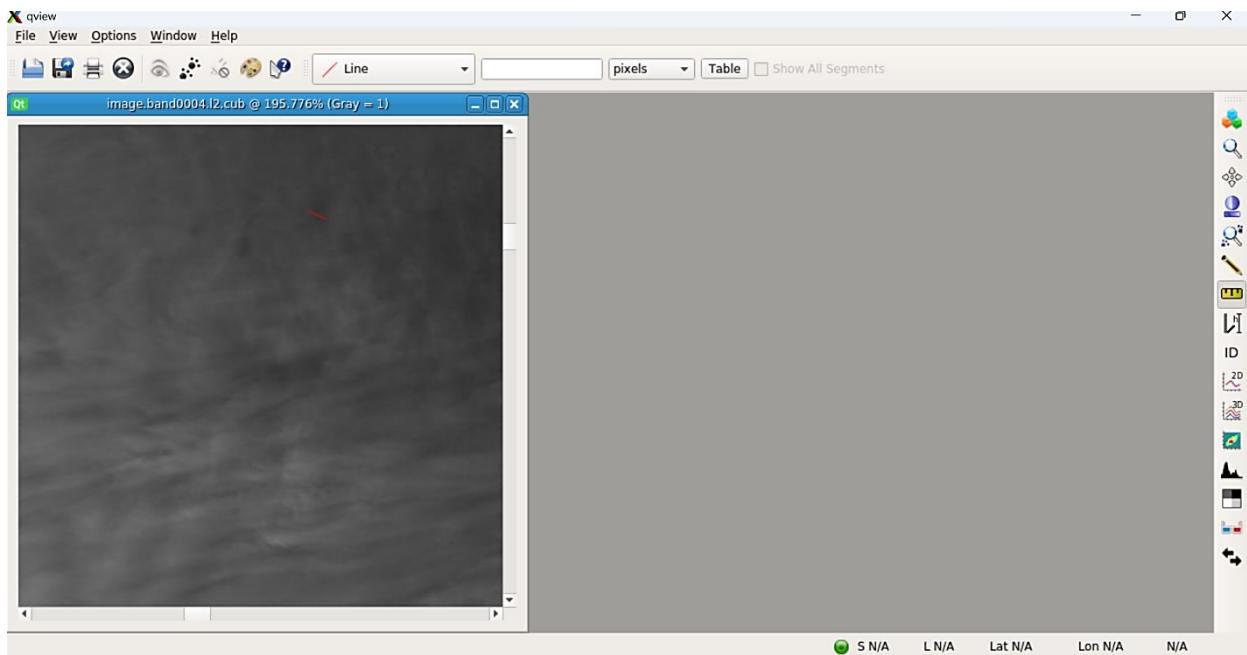


Figure 19: The counting of the pixels according to the Sun Azimuth Angle and the Sun clock.

2.1.5 Calculations of the Height of the Dust Storm

After calculating the shadow lengths, I began calculating the shadow lengths at different points and obtaining the incidence angle at the same points in order to calculate the dust height at each point using the equation below in Figure 20.

$$\text{Height of Dust Storm} = \frac{\text{Shadow length}}{\tan(i)}$$

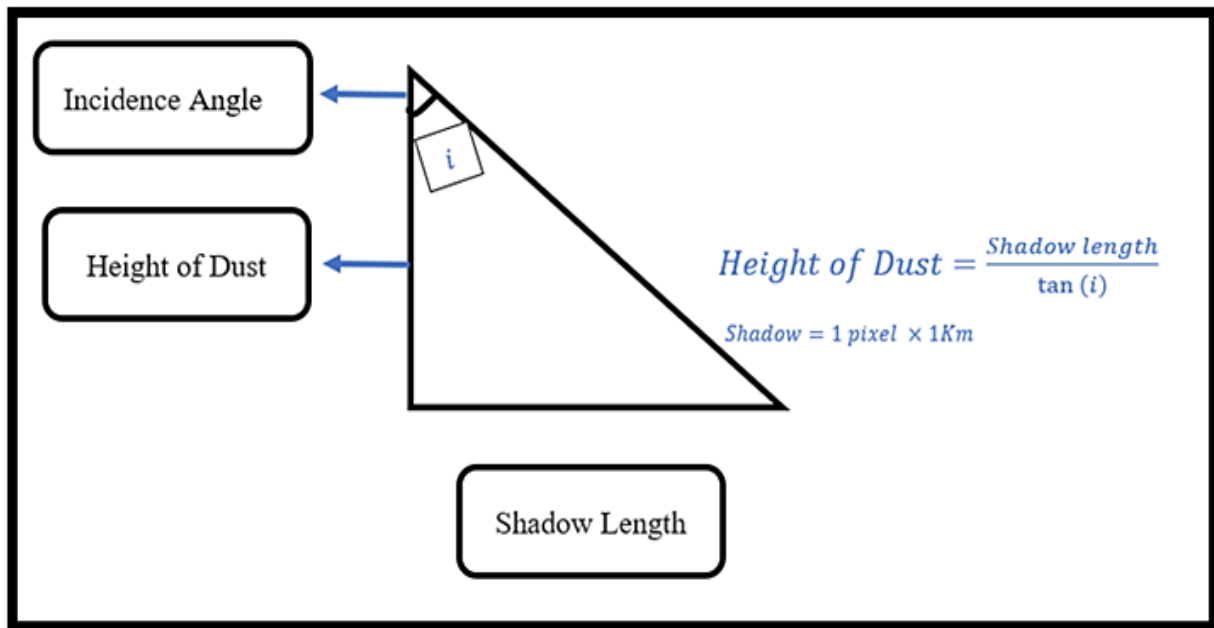


Figure 20: The equation used for calculating the height of the dust storm.

Chapter 3: Results and Discussions

This chapter includes the results of the work done above with PYTHON and QGIS. Both were used to plot the local dust storms' heights associated with each longitude and latitude. Then, numerous forms of visualizations were created.

3.1 Overview of the Main Findings

3.1.1 Table with Needed Parameters for the Visualization

Finally, after calculating 58 points using Equation 1 from Chapter 2 section 2.1.5, the heights of the dust associated with the Longitudes and Latitudes of the first local dust storm which occurred on 20 May 2020. Also, the used parameters in the calculations were provided in Table 1.

Table 1: The Parameters Needed for the Incremental Dust Storm Height of the Local Dust Storm from 20 May 2020.

Point Number	Longitude	Latitude	Sun azimuth angle	Incidence angle	Shadow length	Dust Total Height
1	-24.0226	31.1253	151.91 degree	66.64 degree	25.4391 km	10.98 km
2	-18.5673	31.9423	144.10 degree	71.04 degree	37.6891 km	12.94 km
3	-26.4095	27.5998	148.04 degree	62.35 degree	38.7348 km	20.29 km
4	-31.0676	30.2154	120.37 degree	60.54 degree	33.1971 km	18.75 km
5	-27.2426	31.5762	147.06 degree	63.91 degree	76.3877 km	37.40 km
6	-16.1224	32.9382	130.31 degree	73.36 degree	105.663 km	31.57 km
7	-25.1585	29.0055	148.45 degree	64.50 degree	48.5609 km	23.16 km
8	-15.9167	33.9474	144.18 degree	74.01 degree	57.6692 km	16.52 km
9	-15.0844	33.2010	126.18 degree	74.46 degree	35.7831 km	9.950 km
10	-12.8231	31.7961	128.73 degree	75.65 degree	51.9872 km	13.29 km
11	-13.2137	28.9972	104.46 degree	73.71 degree	45.9861 km	13.43 km
12	-17.3120	29.8533	138.55 degree	71.05 degree	71.4597 km	24.53 km
13	-21.8871	29.5350	154.52 degree	67.93 degree	45.6953 km	18.52 km
14	-17.8221	30.8710	148.78 degree	71.16 degree	42.8877 km	14.63 km
15	-32.3591	28.9423	120.04 degree	58.88 degree	53.5632 km	32.37 km
16	-24.0771	33.0364	151.10 degree	67.62 degree	39.5799 km	16.29 km
17	-26.8822	30.6985	142.25 degree	64.18 degree	29.2409 km	14.14 km

Table 1: The Parameters Needed for the Incremental Dust Storm Height of the Local Dust Storm from 20 May 2020 (Continued).

Point Number	Longitude	Latitude	Sun azimuth angle	Incidence angle	Shadow length	Dust Total Height
18	-29.4339	31.9278	129.18 degree	63.17 degree	33.1360 km	16.75 km
19	-30.1234	30.4900	138.37 degree	61.61 degree	19.0016 km	10.26 km
20	-32.2032	30.5009	115.47 degree	60.21 degree	24.4561 km	14.00 km
21	-18.4927	29.3924	144.72 degree	69.89 degree	64.1594 km	23.49 km
22	-24.8304	28.8765	150.28 degree	64.58 degree	49.1883 km	23.37 km
23	-25.8216	25.3532	153.89 degree	61.94 degree	34.4328 km	18.35 km
24	-23.4109	27.0874	155.03 degree	64.72 degree	19.7873 km	9.340 km
25	-19.9029	25.8171	155.07 degree	66.95 degree	55.8909 km	23.78 km
26	-18.6538	25.5256	158.08 degree	67.89 degree	94.5392 km	38.40 km
27	-28.8534	24.6740	140.84 degree	59.20 degree	72.1762 km	43.02 km
28	-29.4747	27.0295	139.43 degree	60.27 degree	51.0589 km	29.15 km
29	-30.2628	25.2176	120.47 degree	58.44 degree	36.4538 km	22.39 km
30	-29.5633	24.1304	138.06 degree	57.83 degree	32.2209 km	20.26 km
31	-32.9064	26.3772	116.40 degree	57.17 degree	32.8590 km	21.20 km
32	-28.4449	28.6181	142.27 degree	61.63 degree	15.2785 km	8.250 km
33	-28.5678	27.7978	131.26 degree	61.30 degree	36.0120 km	19.71 km
34	-27.9743	26.3881	135.39 degree	60.88 degree	18.5807 km	10.35 km
35	-27.8099	27.6953	137.17 degree	61.64 degree	24.4163 km	13.17 km
36	-23.5042	27.1681	155.02 degree	64.84 degree	27.6445 km	12.98 km
37	-25.8172	24.1250	149.94 degree	61.34 degree	24.8428 km	13.57 km
38	-24.4603	25.7618	154.70 degree	63.21 degree	78.3962 km	39.58 km
39	-26.5988	26.4995	142.86 degree	61.94 degree	37.3799 km	19.92 km
40	-22.5625	25.4044	155.39 degree	64.59 degree	39.2085 km	18.62 km
41	-17.3577	26.7992	149.95 degree	69.42 degree	26.9519 km	10.11 km
42	-17.6047	30.4878	139.84 degree	70.97 degree	22.9579 km	7.918 km
43	-16.1715	30.4736	133.14 degree	72.17 degree	55.8268 km	17.95 km
44	-15.8887	28.9548	132.09 degree	71.70 degree	20.1764 km	6.670 km
45	-21.6162	34.3033	150.37 degree	69.92 degree	20.7985 km	7.902 km
46	-26.1307	32.7436	145.85 degree	65.80 degree	21.1975 km	9.526 km
47	-22.5686	25.4205	155.30 degree	64.62 degree	34.5556 km	16.39 km
48	-25.0192	25.1015	148.66 degree	62.38 degree	24.1149 km	12.61 km

Table 1: The Parameters Needed for the Incremental Dust Storm Height of the Local Dust Storm from 20 May 2020 (Continued).

Point Number	Longitude	Latitude	Sun azimuth angle	Incidence angle	Shadow length	Dust Total Height
49	-29.0093	24.8947	128.83 degree	59.09 degree	41.9122 km	25.09 km
50	-29.7007	24.2143	138.20 degree	58.27 degree	29.4193 km	18.19 km
51	-23.5126	30.4935	152.78 degree	66.43 degree	23.4480 km	10.22 km
52	-27.3514	28.8871	138.63 degree	62.72 degree	14.7417 km	7.600 km
53	-22.5032	26.5611	154.94 degree	65.19 degree	13.5889 km	6.281 km
54	-26.2916	24.7595	142.36 degree	61.30 degree	61.8949 km	33.88 km
55	-26.7491	27.5283	142.53 degree	62.41 degree	29.2832 km	15.30 km
56	-26.5876	26.5876	144.44 degree	62.26 degree	29.6318 km	15.58 km
57	-26.0509	25.7958	144.57 degree	61.99 degree	18.5957 km	9.891 km
58	-28.9486	33.0763	132.93 degree	64.10 degree	40.5421 km	19.68 km

The table below illustrates in 66 points the parameters required to visualize the second local dust storm, which occurred on June 8, 2021 (Table 2):

Table 2: The Parameters Needed for the Incremental Dust Storm Height of the Local Dust Storm from 8 June 2021.

Point Number	Longitude	Latitude	Sun azimuth angle	Incidence angle	Shadow length	Dust Total Height
1	134.862	54.500	54.580 degree	46.24 degree	12.2109 km	11.96 km
2	132.876	58.181	58.092 degree	47.52 degree	9.25129 km	8.471 km
3	127.616	56.448	56.660 degree	44.49 degree	31.6007 km	32.16 km
4	136.650	57.079	57.480 degree	48.97 degree	22.6327 km	19.69 km
5	137.636	56.726	56.777 degree	48.70 degree	15.3572 km	13.49 km
6	137.745	57.197	57.090 degree	48.94 degree	23.0358 km	20.06 km
7	137.636	56.220	56.230 degree	48.78 degree	20.7221km	18.15 km
8	137.921	59.346	59.470 degree	50.36 degree	16.3570 km	13.55 km
9	133.736	57.740	58.000 degree	47.67 degree	17.9979 km	16.39 km
10	143.526	60.944	60.995 degree	53.72 degree	35.3713 km	26.54 km
11	143.218	59.602	59.546 degree	53.11 degree	28.7695 km	21.59 km
12	138.534	59.476	59.590 degree	50.68 degree	35.6761 km	29.22 km
13	137.024	57.518	57.559 degree	48.99 degree	24.9186 km	21.66 km

Table 2: The Parameters Needed for the Incremental Dust Storm Height of the Local Dust Storm from 8 June 2021 (Continued).

Point Number	Longitude	Latitude	Sun azimuth angle	Incidence angle	Shadow length	Dust Total Height
14	142.757	56.540	56.409 degree	51.25 degree	31.0654 km	24.93 km
15	140.520	56.330	56.380 degree	50.14 degree	22.3771 km	18.68 km
16	139.262	56.134	56.122 degree	49.39 degree	28.7695 km	24.66 km
17	144.980	58.078	58.087 degree	53.00 degree	24.6414 km	18.56 km
18	141.624	57.882	57.457 degree	51.24 degree	24.1344 km	19.37 km
19	138.534	59.476	55.927 degree	48.06 degree	22.8629 km	20.54 km
20	139.751	58.022	58.133 degree	50.50 degree	33.5323 km	27.64 km
21	135.920	56.735	56.669 degree	48.08 degree	37.8345 km	33.97 km
22	134.046	55.938	56.120 degree	46.67 degree	27.7981 km	26.22 km
23	136.507	55.169	55.280 degree	47.80 degree	28.2272 km	25.59 km
24	136.479	56.763	56.572 degree	48.25 degree	14.2589 km	12.72 km
25	140.156	56.484	56.405 degree	49.96 degree	24.0917 km	20.24 km
26	134.102	56.652	65.691 degree	47.11 degree	24.0917 km	22.37 km
27	118.057	55.069	55.640 degree	39.58 degree	32.1723 km	38.91 km
28	123.559	54.192	55.572 degree	41.30 degree	25.9885 km	29.58 km
29	124.282	54.104	54.130 degree	41.17 degree	31.2943 km	35.70 km
30	127.243	55.760	55.948 degree	43.81 degree	27.1285 km	28.27 km
31	132.887	56.821	56.978 degree	46.80 degree	30.3980 km	28.54 km
32	130.813	54.940	54.701 degree	44.57 degree	26.3642 km	26.76 km
33	126.085	55.664	55.864 degree	43.05 degree	38.3656 km	41.07 km
34	139.304	57.979	57.866 degree	50.19 degree	28.596 km	23.83 km
35	129.414	57.129	57.345 degree	45.41 degree	30.398 km	29.96 km
36	134.238	56.966	57.006 degree	47.44 degree	23.5809 km	21.65 km
37	125.989	54.795	54.683 degree	42.35 degree	32.3527 km	35.49 km
38	119.524	58.076	58.736 degree	41.55 degree	26.9774 km	30.43 km
39	117.401	54.892	55.719 degree	39.60 degree	38.8948 km	47.01 km
40	134.758	57.641	57.809 degree	48.18 degree	38.7591 km	34.67 km
41	138.708	56.064	56.050 degree	49.04 degree	25.9374 km	22.51 km
42	141.063	57.270	57.182 degree	50.66 degree	30.7573 km	25.21 km
43	133.841	57.557	57.505 degree	47.56 degree	31.1718 km	28.50 km
44	136.966	54.136	53.896 degree	47.15 degree	20.6849 km	19.18 km
45	124.191	54.062	54.120 degree	41.03 degree	35.4858 km	40.77 km

Table 2: The Parameters Needed for the Incremental Dust Storm Height of the Local Dust Storm from 8 June 2021 (Continued).

Point Number	Longitude	Latitude	Sun azimuth angle	Incidence angle	Shadow length	Dust Total Height
46	133.341	56.899	56.579 degree	47.06 degree	28.8475 km	26.84 km
47	118.666	56.732	57.505 degree	41.15 degree	27.6558 km	31.64 km
48	115.301	56.389	57.852 degree	40.83 degree	30.1776 km	12.61 km
49	122.680	53.812	53.314 degree	40.54 degree	28.6585 km	33.50 km
50	118.543	56.896	57.577 degree	41.78 degree	17.9457 km	20.08 km
51	119.204	54.620	54.998 degree	40.08 degree	24.6213 km	29.25 km
52	131.540	55.795	55.919 degree	45.66 degree	13.9347 km	13.61 km
53	124.785	56.529	56.173 degree	43.51 degree	28.3746 km	29.89 km
54	135.836	53.739	53.865 degree	46.46 degree	21.5436 km	20.47 km
55	128.383	55.685	55.892 degree	44.09 degree	22.4057 km	23.12 km
56	130.218	57.043	57.443 degree	45.69 degree	20.5305 km	20.04 km
57	141.673	56.896	56.929 degree	50.91 degree	14.5986 km	11.85 km
58	146.813	58.732	58.973 degree	54.26 degree	21.7623 km	15.66 km
59	148.502	56.603	56.920 degree	54.25 degree	20.6455 km	14.86 km
60	142.848	58.108	57.082 degree	51.53 degree	15.693 km	12.69 km
61	147.180	60.201	60.252 degree	54.83 degree	23.1337 km	16.30 km
62	149.016	57.520	57.518 degree	54.89 degree	24.8129 km	17.44 km
63	135.872	58.732	58.410 degree	49.17 degree	19.4648 km	16.81 km
64	116.487	56.529	56.448 degree	40.56 degree	15.6930 km	18.33 km
65	122.508	55.354	56.001 degree	41.91 degree	25.379 km	28.27 km
66	117.442	60.421	61.120 degree	43.85 degree	15.3883 km	16.01 km

All the steps in Chapter 2 assisted in identifying the various parameters needed to visualize the chosen local dust storms, such as incidence angle and sun azimuth angle at each point within the local dust storm. Furthermore, the dust shadow length estimated from the image was computed. Then, using the equation from Chapter 2, the most important aspect of the dust storm, its incremental height, was calculated.

For the first dust storm, the dust gradually expanded westward, reaching a maximum height of around 43 km at point 27, according to calculations from (Table 1). As calculated for the second dust storm, the local dust storm reached a maximum height of around 47 km at point 39 (Table 2). Therefore, the second dust storm was nearly 4 km higher than the first.

In the end, the results of the work were summarized and presented in Tables 1 and 2, which included all the necessary parameters.

3.1.2 Determine the Horizontal Expand of the Local Dust Storm

The horizontal expansion of the local dust storm was estimated using ISIS. First, viewing the local dust storm image was accomplished using the QVIEW command. Simply then, the local dust storm horizontal dust expansion was estimated using the ruler line indicator that indicates each pixel equals 1 km as I set the resolution previously in Chapter 2 Section 2.1.3 to 1 km per pixel. Therefore, according to the red line length that crosses the local dust storm from the start of dust appearances on the image to the end, the May 20, 2020, local dust storm, has a horizontal extent of around 1200 km (Figure 21).

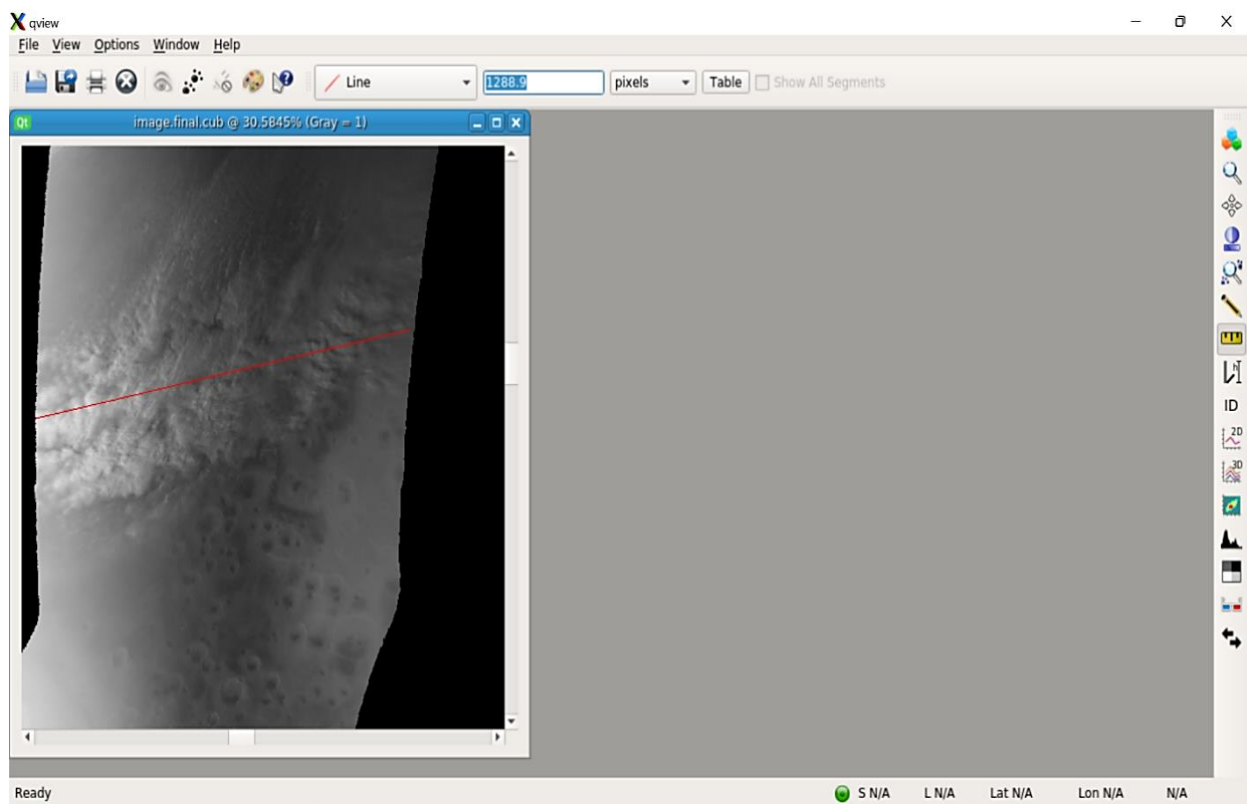


Figure 21: The horizontal expand from center of the local dust storm on 20 of May 2020.

The same procedures were followed for the second local dust storm, which occurred on June 8, 2021, with a horizontal extent of around 1700 km (Figure 22).

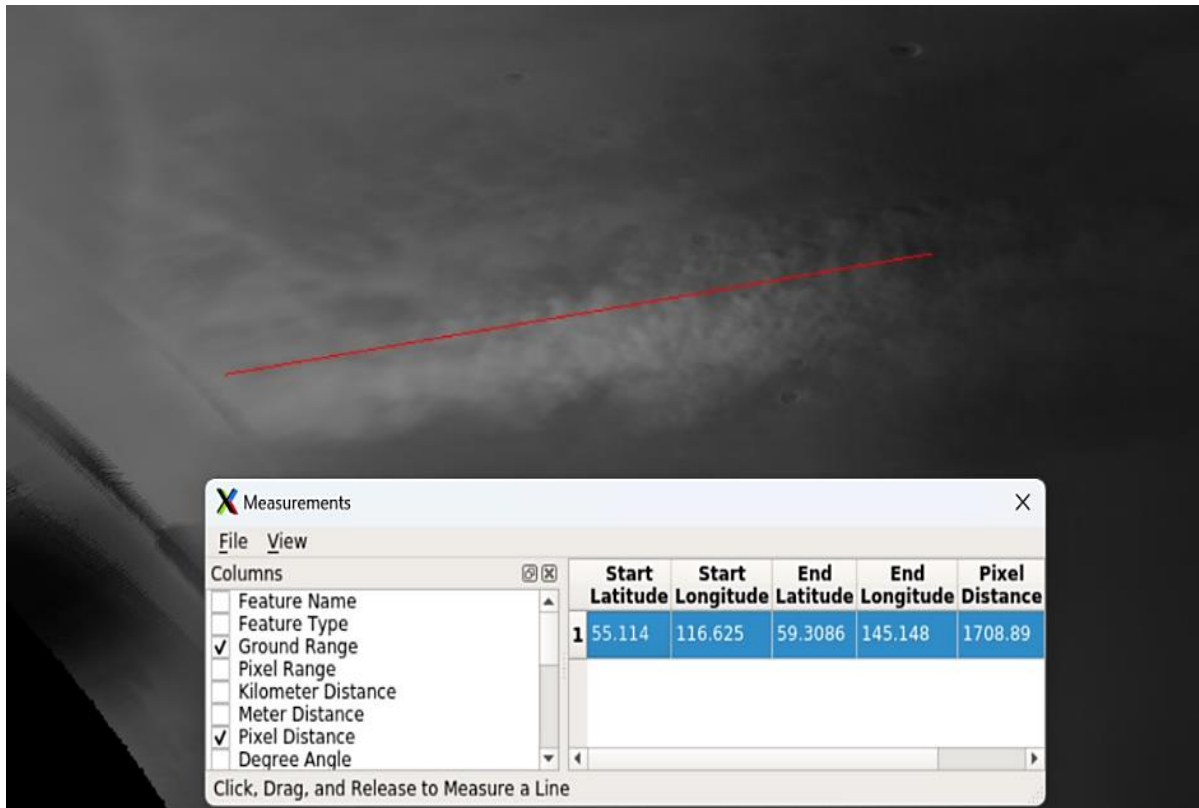


Figure 22: The horizontal expand from center of the local dust storm on 6 of June 2021.

The length and expansion of local dust storms on Mars are important features to consider when studying them. Local dust storms are typically smaller in size and extent than regional or global dust storms, but they can still have significant effects on the Martian environment.

In this context, the second dust storm, which is 500 km longer than the first, is still considered a local dust storm because its length is less than 2000 km.

It is worth noting that the length and expansion of local dust storms can vary widely. Some local dust storms may be only a few hundred km long, while others can stretch for thousands of km. The intensity of the storm can also vary, with some producing only a light coating of dust and others causing thick dust clouds that obscure the surface of the planet.

In addition, the smaller size and limited scope of local dust storms make them ideal targets for detailed study and analysis. By studying the length and expansion of local dust storms on Mars, researchers can also gain insights into the mechanisms that drive them. For example, changes in temperature or atmospheric pressure can create areas of instability that lead to the formation of local dust storms. By understanding these mechanisms, scientists can develop more accurate models of the Martian atmosphere and improve their ability to predict the behavior of dust storms on the planet.

3.1.3 Three-Dimensional Visualization using PYTHON

The below visualizations were produced using PYTHON, Tables 1 and 2 data. PYTHON Visualizations technique utilizes the use of both Matplotlib and NumPy packages.

3.1.3.1 Three-Dimensional Visualization of the Dust Storm Heights Distribution

The first result was a 3D visualization of the point distribution (dust height with each longitude and latitude) from Tables 1 and 2.

For the first dust storm, the distribution of the points indicates the maximum height of the dust storm, which is 43.02 km at -28.8534 longitudes and 24.6740 latitudes, and the lowest height, which is 6.281 km at -22.5032 longitudes and 26.5611 latitudes (Figure 23).

20 of May 2020 Dust Storm Height 3D Visualization

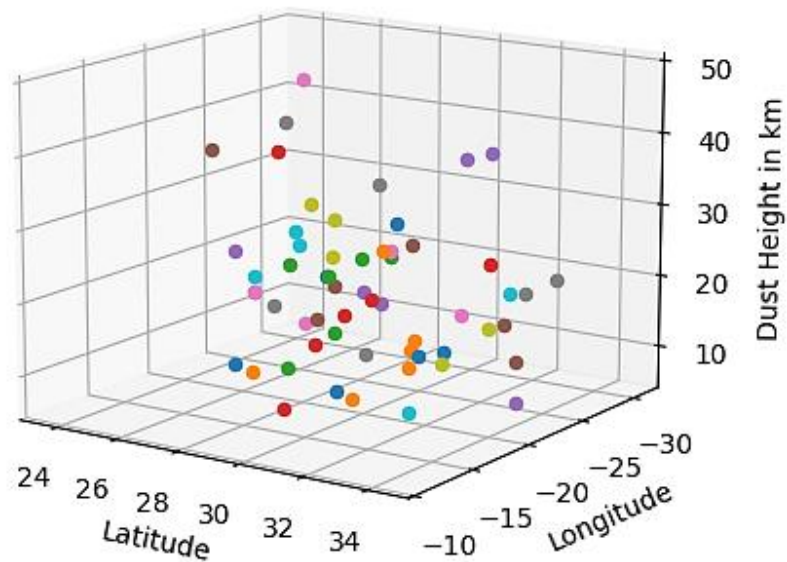


Figure 23: The distribution of height within the first local dust storm.

The distribution of height for the second dust storm demonstrates that the dust storm's maximum height is 47.01 km at 117.401 longitude and 54.892 latitudes, and its lowest height is 8.471 km at 132.876 longitude and 58.181 latitude (Figure 24).

8 of June 2021 Dust Storm Height 3D Visualization

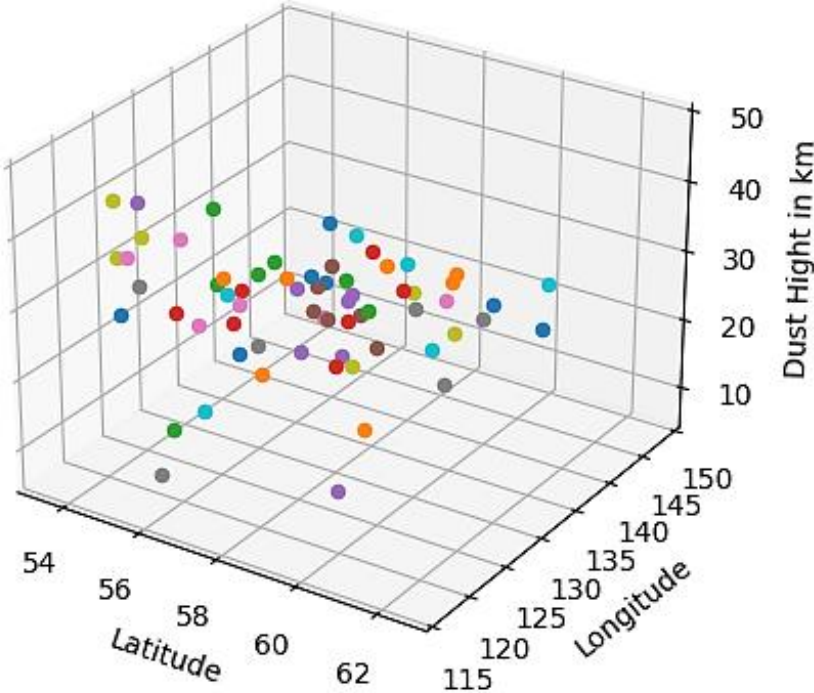


Figure 24: The distribution of height within the second local dust storm.

3.1.3.2 The Contour Map Represents the Heights of Dust

The result produces contour maps of the various dust heights within the two local dust storms. Lower heights are indicated by darker blue areas, while higher dust lifting is indicated by deeper red spots (Figure 25). Both depicted that local dust storms have higher dust-lifting heights on the western side than on the eastern side. The western side has both dust storm peaks and is mostly green, yellow, and some red, whereas the eastern side is mostly dark blue, indicating a lower dust height.

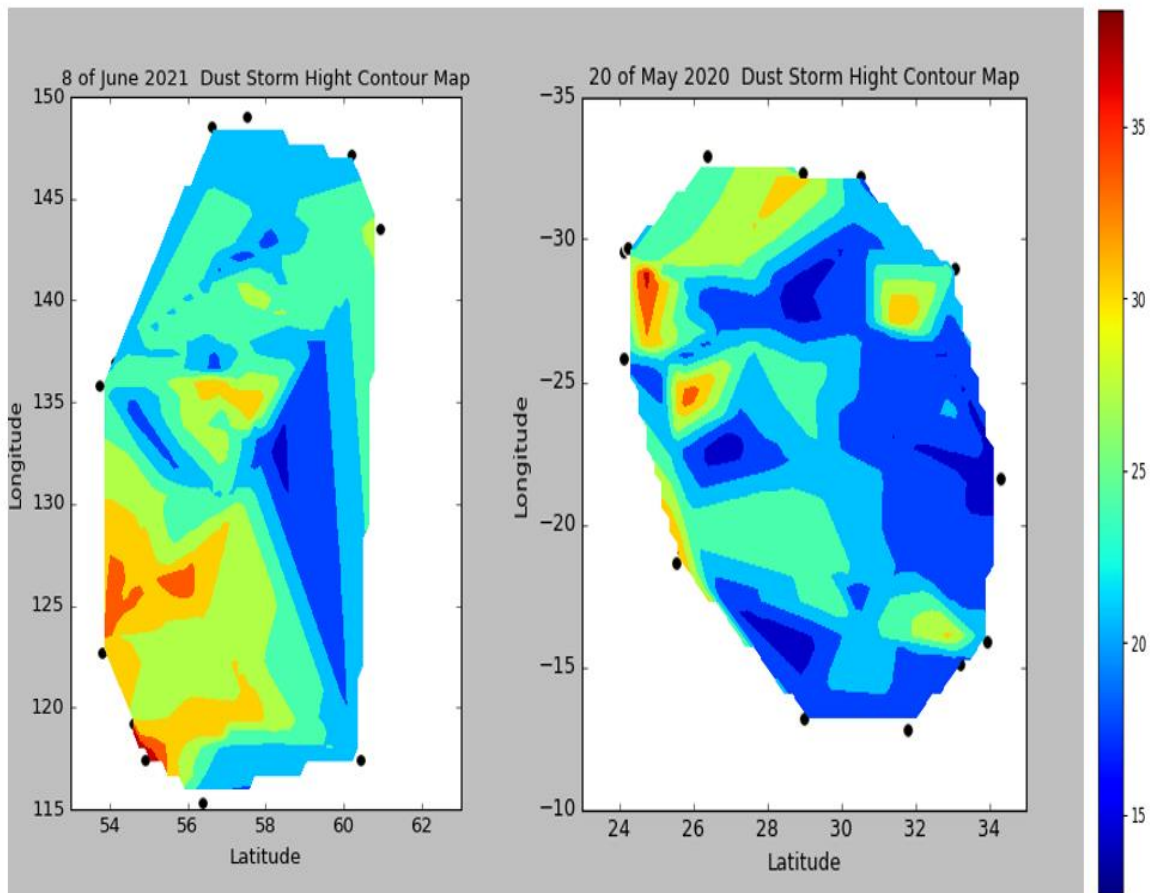


Figure 25: A contour maps of both local dust storms represents the heights of dust.

3.1.4 The QGIS Three-Dimensional Visualizations

3.1.4.1 Three-Dimensional Visualization using QGIS qgis2threejs Exporter

This result aims to document the process of analyzing and visualizing the dust storm heights on Mars using QGIS tools. The data used in this analysis includes Tables 1 and 2. and a Digital Elevation Model (DEM) of Mars.

3.1.4.1.1 Preparing the Needed Requirements for the QGIS Visualization

The first step was to obtain the necessary data. A Mars DEM was downloaded from PDS, the DEM was based on data from MOLA an instrument from the MGS spacecraft. This MOLA\DEM represents more than 600 million measurements gathered between 1999 and 2001 (MOLA, 2020) .



Figure 26: A Mars DEM from MOLA\ MGS.

Dust storm heights measurements were obtained from. These measurements were recorded in an Excel file with three columns: latitude, longitude, and dust storms heights were converted to meters because the DEM elevations were in meters. The data was then imported into QGIS as a point layer. The next step was to clip the DEM to the study areas. The two dust storms are shown below in Figures 27 and 28.

20 May 2020 Local Dust Storm Area

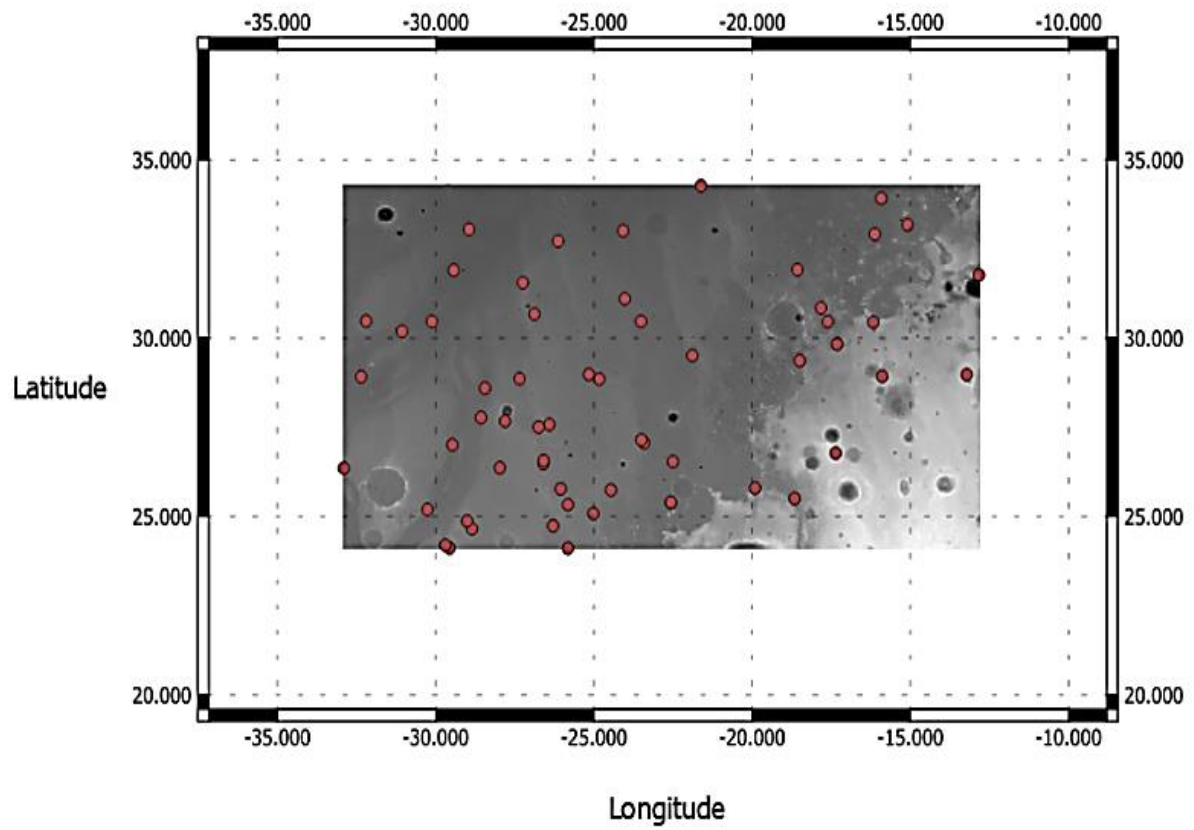


Figure 27: The map displays the DEM of the study area, as well as the distribution of the dust Heights from the local dust storm on May 20, 2020.

8 June 2021 Local Dust Storm Area

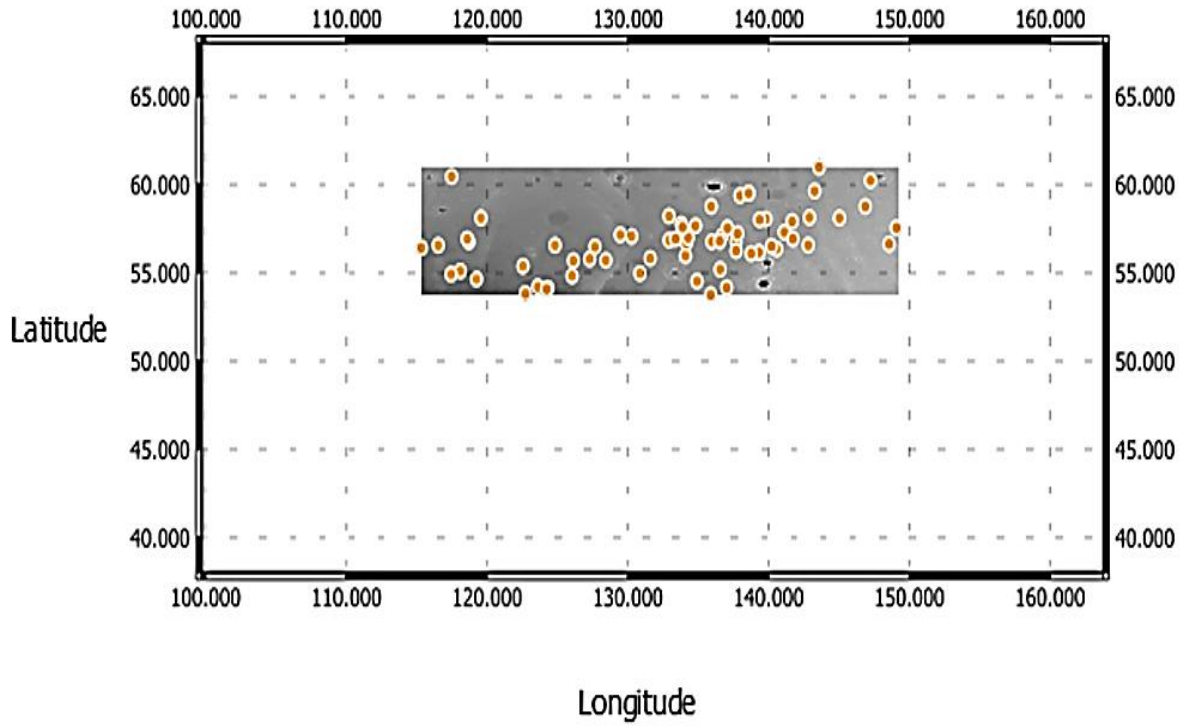


Figure 28: The map displays the DEM of the study area, as well as the distribution of the dust Heights from the local dust storm on June 8, 2021.

Following that, both dust storm DEM areas were converted to points using the function Raster pixels to point. That helped in determining the spatial information of the study areas including the existing elevations. Then, the dust storm's height points from Tables 1 and 2. were buffered to a radius of 0.5, and the resulting polygons were used to be added to the existing elevation values from the DEM. This was achieved by using the “Join by Attribute Location” tool in QGIS, which added an elevation value to each dust storm height point based on the DEM value at that location. The resulting layer contained four fields: latitude and longitude for the dust storm's heights, and existing elevations.

To analyze the data, the elevation and dust storm height values were combined into a single field using “field calculator” from the newly generated layer attribute table, and the following conditional statement:

CASE

WHEN "VALUE_2" IS NOT NULL THEN ("VALUE" + "VALUE_2")

ELSE "VALUE"

END

The conditional statement above was imported into the "field calculator". Therefore, if a dust storm's height points had a corresponding elevation value, the two values were added together. If there was no elevation value matching with the dust storms height points the value of the existing elevation would remain. Now, the layer contained both the elevations and dust storm height information in a single value. All the values were then converted from m to km using the “field calculator” The following was imported in the “field calculator” and applied for the field:

"VALUE" \ 1000

Finally, to visualize the data, the dust storm's height layers were rasterized using the “Rasterize (Vector to Raster)” tool in QGIS. The horizontal and vertical resolutions were set to 1000 m to produce a grid that accurately represented the study area. The resulting raster images contained elevation and dust storm height values in each pixel in Figures 29 and 30.

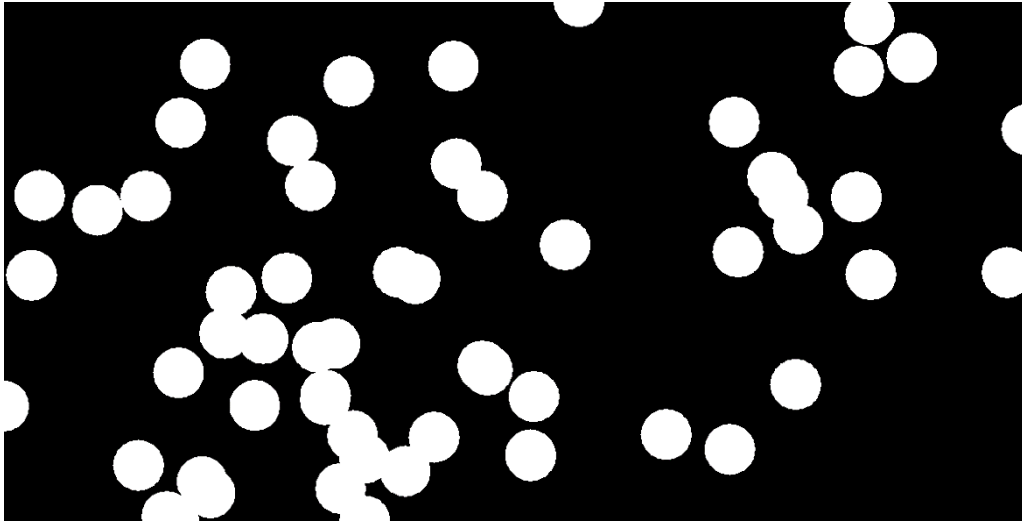


Figure 29: The representative raster image for 20-5-2020 local dust storm

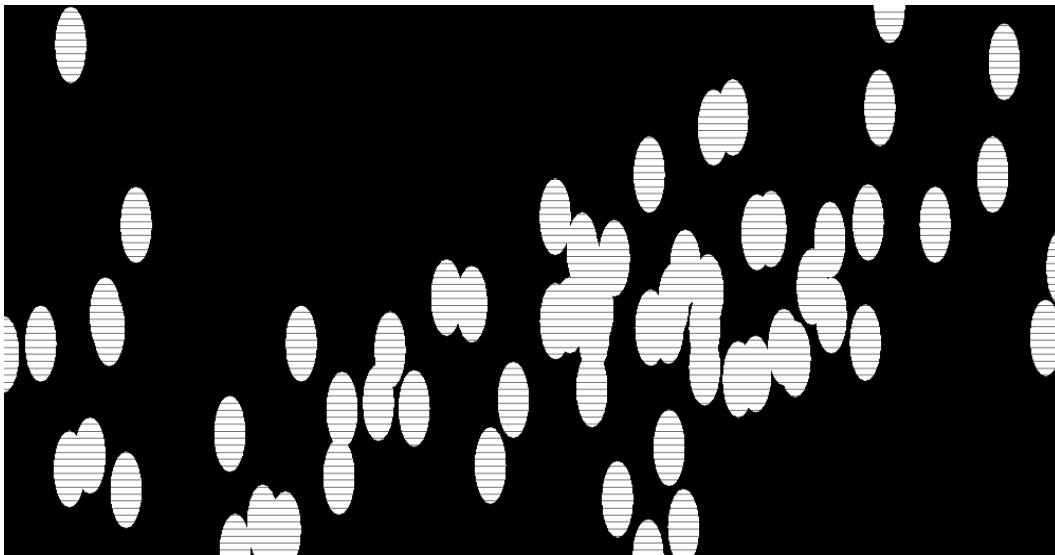


Figure 30: The representative raster image for 8-6-2021 local dust storm

Then, using the Georeferencer tool from the Raster functions, an image of the local dust storms from the Meteo Mars tool Figures 31 and 32 and an effect of dust above the images were Georeferenced using the "From Map Canvas" function. The georeferencing was done using layers that had already been created, such as the local dust storm new raster layer.



Figure 31: 20 of May 2020 local dust storm from MeteoMars MARCI\MRO with a dust effect.



Figure 32: 8 of June 2021 local dust storm from MeteoMars MARCI\MRO with a dust effect.

3.1.4.1.2 *Producing Three-Dimensional Visualization using QGIS qgis2threejs Exporter*

Finally, the raster images were visualized in QGIS using the qgis2threejs tool. This tool allowed for the creation of an interactive 3D visualization that displayed both the existing elevations and dust storm height values. The resulting visualization revealed two distinct dust storms: one on May 20, 2020, in the Chryse Planitia Region of Mars, and the other on June 8, 2021, on the northern side of the Utopia Planitia Region

The scenes were run with a suitable Z exaggeration, for the first dust was on 0.003 to give the visualization a smoother look. The Z exaggeration parameter is useful when the Z units differ from the X and Y units, it will affect the terrain shape and Z positions of all vector 3D objects. Note: In the three-dimensional visualization, the yellow dot in the storm represents longitude, latitude, and elevation. As illustrated in the upper left box, the viewing directions are indicated by colored dots on the right lower side (Figures 33 and 34). The visualizations indicate the texture, dust heights, and shape of the local dust storms:

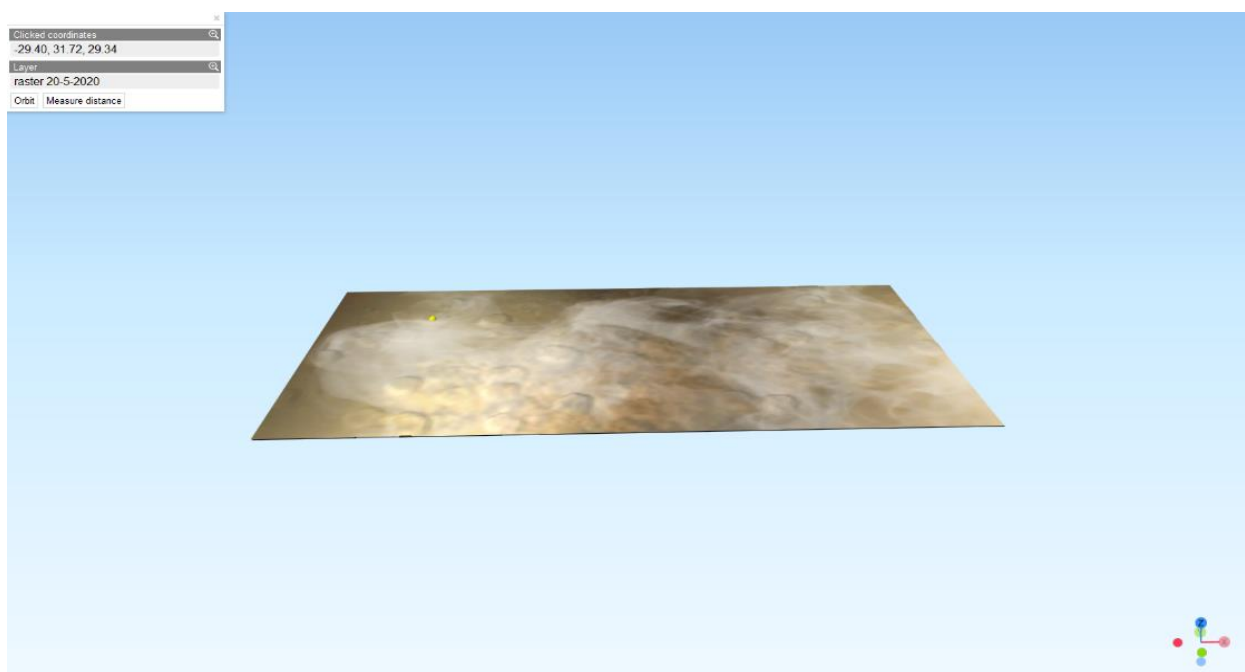


Figure 33: 3D visualization of 20 -5-2020 local dust storm.

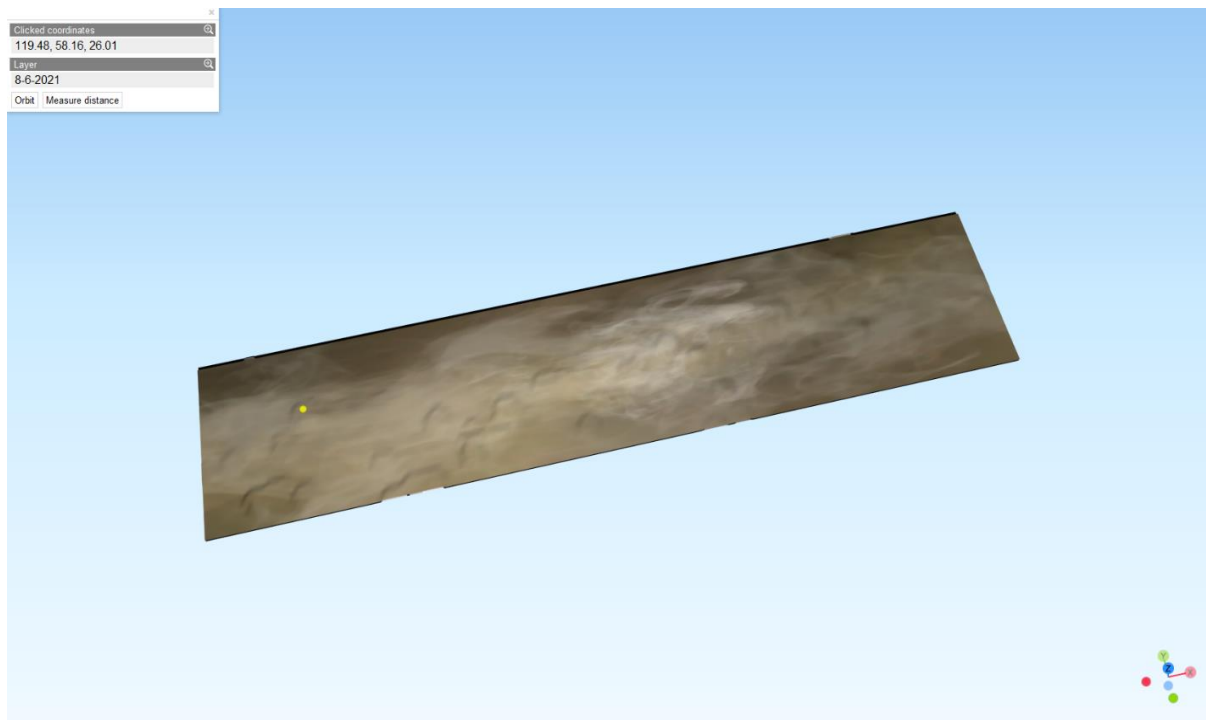


Figure 34: 3D visualization of 8 -6-2021 local dust storm.

All the above outlined the process of analyzing and visualizing dust storm heights on Mars using QGIS tools. The process involved importing and manipulating data, clipping, and joining layers, combining data fields, rasterizing the layer, and visualizing the data in 3D. The resulting visualizations provided valuable insights into the dust storms on Mars and demonstrated the capabilities of QGIS tools in analyzing and visualizing dust storm data.

All the results represent the main features of the local dust storms that occurred back on 20 May 2020 and 8 June 2021 from MARCI\MRO. The dust heights were projected on several visualizations indicating the height, shape, and texture.

As a result of the calculations and the image's projected shadows. The visualizations of the first local dust storm demonstrate the vertical spread of dust heights ranging from 5 to 43 km. Aside from that, the horizontal spread has been approximately 1200 km. Furthermore, the second dust storm's vertical spread heights varied from 8 to 47 km, with a horizontal spread of around 1700 km, all the visualizations above indicating that the results are mostly representative of local dust storms.

Several factors can affect the height of local dust storms on Mars, including the strength and direction of the winds, the amount of dust and sand available to be lifted, and the atmospheric conditions. In general, stronger winds and more dust and sand can lead to higher dust storm heights.

Dust storms on Mars are driven by the planet's strong winds. The stronger the winds, the more dust and sand can be lifted, and the higher the resulting dust storm can reach. The direction of the winds can also play a role in the height of the storm, as winds blowing in a more upward direction can lead to higher plumes (Leovy C. E., 1973).

In terms of the elevation variety, in both Chryse Planitia and Utopia Planitia the locations of the local dust storms that have been visualized in this work are relatively flat and have a limited range of elevations compared to other regions on Mars. However, Utopia Planitia has a slightly higher elevation range than Chryse Planitia. Therefore, the topography of the region where the local dust storms form can have a direct effect on the dust height. Regions with steep terrain or canyons can cause the winds to accelerate, leading to stronger lifting forces and higher dust storm heights. That might be the reason why the second dust storm dust height was higher than the first one (Smith, 1999).

Further, the temperature and pressure of the Martian atmosphere can also affect the height of local dust storms. Warmer temperatures and lower atmospheric pressure can lead to higher dust storm heights, as the lower atmospheric pressure allows the dust and sand to be lifted more easily (Leovy C. B., 1979).

There is currently no available data specifically comparing the size of dust particles between the Chryse Planitia region and the Utopia Planitia region on Mars. However, it is generally known that Martian dust particles range in size from less than 1 μm to several μm in diameter, with some larger particles up to 10 μm .

The size of dust particles on Mars can vary depending on several factors, including local geology, weather patterns, and the presence of wind and other atmospheric conditions. Factors such as these could potentially result in variations in dust particle size between different regions of the planet, including Chryse Planitia and Utopia Planitia.

Therefore, without specific data on the size of dust particles in these two regions, it is difficult to make a direct comparison. However, the dust particles in these regions are generally similar in size to those found elsewhere on the planet, with variations depending on local conditions.

In general, local dust storms on Mars can reach heights of several km, with the largest ones reaching up to 60 km in height as Chapter 1 Section 1.4.4 indicates. However, the height of a dust storm can vary depending on the specific conditions present in the region where it forms.

Chapter 4: Conclusion

This work highlighted how the dust heights of the dust storm were calculated from its shadow using various methods, tools, and software such as ISIS, QGIS, MeteoMars, and PYTHON. In addition, three-dimensional visualizations of the selected local dust storms were generated.

Further, the first dust storm that occurred on 20 May 2020 which relevant to 35 MY in the northern hemisphere at the Chryse Planitia region of Mars. According to the findings, this work indicated that the dust storm has extant horizontally around 1200 km and vertically from the height calculations by around 5km to 40 km. Furthermore, the second dust storm occurred on 8 June 2021, which is relevant to 36 MY located beside the northern side of Mars's Utopia Planitia region. Depending on the findings, this local dust storm has an extent horizontally by 1700 km and vertically by around 8 to 45 km according to the calculations.

In this work, all the visualizations for the first local dust storm indicate that the dust was concentrated on the north-western side of the dust storm. Therefore, the dust storm height was increased towards the northwest and that may happen because of the surface dust lifted by the wind. On this side, the highest values of dust heights were centralized mostly around -24 to -29 longitudes. On the other hand, the lowest values were on the eastern side of the dust storm almost at -15 to -23 longitude, this dust storm reached the maximum height of the dust at 43.02 km at -28.8534 longitude and 24.6740 latitudes, and the lowest was around 6.281 km at -22.5032 longitude and 26.5611 latitudes. For the second local dust storm, the vertical spread was toward the southwestern side of the dust storm, with the highest values concentrated relatively around 115 to 130 degrees east and the lowest values above 130 degrees east, and it reached the maximum height of the dust of 47.01 km at 117.401 longitudes and 54.892 latitudes, and the lowest height was about 8.471 km at 132.876 longitudes and 58.181 latitudes.

After the calculations, a generation of 58 height points for the first dust storm and 66 for the second dust storm from calculating the height from the projected shadows due to the limitation of the shadows within the image those number of points was used for visualizing the local dust storms in several ways. It is important to note that the method estimates the height of the dust storm based on the image's shadows, which could result in some uncertainty in the measurement. Furthermore, this method assumes that the ground beneath the dust storm is flat, which may not always be the case on Mars.

Through this work, the first chapter was an introduction to other chapters. In the first place, this chapter provided a comprehensive overview of the thesis and what the reader needs to understand before proceeding with the other chapters. In addition, emphasize the goals of this work. It also gave a brief description of some of the work's requirements by introducing them under Data Description Section 1.5. Furthermore, this chapter includes variable information about the history of dust storms and scientific exploration. Also, offer some information about the dust activity in both the Chryse Planitia and Utopia Planitia region of Mars, which are the locations of the local dust storms considered in this work.

The methods used in this work were detailed in the second chapter, starting with downloading raw images of local dust storms. Then, the images were processed, and the required parameters were generated. Following that, the image's shadow length was calculated. Following that, the selected dust storm dust heights were calculated.

Chapter 3 generated 2 Tables listing the needed parameters for visualizing the chosen dust storms. Then, demonstrates the generation of three-dimensional visualizations of Mars' dust storms. The visualizations in this chapter enabled a quick determination and understanding of the dust storm, as well as the capacity to evaluate the dust storm's major features and characteristics. For example, the visualizations produced by PYTHON illustrate the height and shape of the chosen Mars dust storms. Furthermore, the QGIS visualizations present a realistic three-dimensional visualization version of the chosen local dust storms, allowing the viewer to determine the dust storm's height, shadow, structure, texture, and direction easily and effectively.

To date, the understanding of dust and dust storm motion on Mars has depended on Earth theory, computer visualizations, and wind tunnel experiments at partial Mars conditions (Newman CE, 2020). Therefore, this work outlines the approach and methodology used to determine dust storm height by analysing its shadow using MARCI/MRO images. MARCI/MRO images provide high-resolution images of the Martian atmosphere. These images are captured at various times of the day, which allows for analysing the dust storm height based on the length of the shadow cast by the dust plume. One of the main advantages of using MARCI/MRO images is their high spatial resolution, which allows researchers to accurately measure the height of the dust storm. However, these images only provided a two-dimensional view of the dust storm, which limits the accuracy of the measurements.

To process the MARCI/MRO images, the study used ISIS, an Integrated Software for Imagers and Spectrometers, which provides image processing and analysis capabilities. However, it requires a certain level of expertise to operate effectively and can be slow when processing large datasets.

The work concludes that the visualization technique created for the three-dimensional visualization of a dust storm on Mars can significantly aid in the understanding of the behaviour and dynamics of dust storms and their impacts on the Martian atmosphere. I intend to utilize other tools and software, such as ENVI and GDAL are two other software systems which can perform some of the functions of ISIS, but they each have their strengths and weaknesses.

Despite the advantages of other image-processing software, ISIS remains the most comprehensive and reliable software system for processing and analysing planetary science data. Its specialized functionality, large user community, and proven reliability make it the gold standard for working with spacecraft imaging data.

Ultimately, I can demonstrate that the work was accomplished due to the suitable methods, tools, and software that were obtained and used to generate the three-dimensional visualizations of the two local dust storms.

References

- Antoniadi, A. (1930). *The planet MARS*. (P. Moore, Trans.) France: Keith Reid Limited Shaldon Devon. Retrieved from <http://mars-exploration.co.uk/docs/Antoniadi-The%20Planet%20Mars-1930.pdf>
- Aoki, S. A. (2019). Water vapor vertical profiles on Mars in dust storms observed by TGO/NOMAD. *Journal of Geophysical Research: Planets*, 124(12), 3482-3497.
- Balme, M. a. (2006). Dust devils on Earth and Mars. *Reviews of Geophysics*.
- Battalio, M. a. (2021). The Mars Dust Activity Database (MDAD): A comprehensive statistical study of dust storm sequences. *Icarus*, 354, 114059.
- Bell III, J. F. (2009). Mars reconnaissance orbiter Mars color imager (MARCI): instrument description, calibration, and performance. *Journal of Geophysical Research: Planets* . Retrieved from MSS: <https://www.msss.com/science/marci-science-objectives.php>
- Briggs, G. A. (1974). Mariner 9 observations of the Mars north polar hood. *Bulletin of the American Meteorological Society* 55.
doi:file:///C:/Users/user/Downloads/1520-0477-1520-0477_1974_055_0278_mootmn_2_0_co_2%20(3).pdf
- Cantor BA, J. P. (2001). Martian dust storms: 1999 Mars orbiter camera observations. *ournal of Geophysical Research: Planets*.
- Cantor, B. A. (2007). MOC observations of the 2001 Mars planet-encircling dust storm. *Icarus*, 186(1), 60-96.
- Carr, M. H. (1980). *Viking orbiter views of Mars*. US Government Printing Office.
- Clancy, T. M. (2006). Mars Weather and Ozone Column Mapping with MRO/MARCI. *In Mars Atmosphere modeling conference. 2006*, (p. 1).
- Cooper, K. (2022). An atmospheric scientist talks with us about the science that drives the Red Planet's dust storms. *space.com*.
- Ferguson, D. C. (1999). Evidence for Martian electrostatic charging and abrasive wheel wear from the Wheel Abrasion Experiment on the Pathfinder Sojourner rove. *Journal of Geophysical Research*. Retrieved from <https://www.nasa.gov/feature/goddard/the-fact-and-fiction-of-martian-dust-storms>
- Forget, F. a. (2017). Atmospheric dust on Mars. *a review. 47th International Conference on Environmental Systems*.

- Forget, F. F.-L.-G.-V. (2009). Density and temperatures of the upper Martian atmosphere measured by stellar occultations with Mars Express SPICAM. *Journal of Geophysical Research*.
- Gebhardt, C. A.-T.-P. (2021). Characterizing dust-radiation feedback and refining the horizontal resolution of the MarsWRF model down to 0.5 degree. *ournal of Geophysical Research*.
- Gerald A. Soffen, A. T. (1972). The viking missions to mars. *Icarus*, 16(1), 1-16. Retrieved from Jet Propulsion Laboratory: https://d2pn8kiwq2w21t.cloudfront.net/documents/viking_YBc3kvY.pdf
- Gertz, M. (2016). This Is the First Photo Ever Taken from the Martian Surface. *Time*.
- Greeley, R. (1991). *Sand and dust on Mars*.
- Grossman, L. (2021). Perseverance will study Mars weather and terrain, but dust storms could pose a challenge. *Science News*.
- Iñaki Ordóñez-Etxeberria, R. H.-L.-R. (2019). Characterization of a local dust storm on Mars with REMS/MSL measurements and MARCI/MRO images. *Icarus*.
- Instrument Description MARCI\MRO*. (2005). Retrieved from Malin Space Science Systems: <https://www.msss.com/mro/marci/description.html>
- ISIS. (2023). Retrieved from Integrated Software for Imagers and Spectrometers: <https://isis.astrogeology.usgs.gov/7.0.0/index.html>
- JD., B. (2001). *Meteorological Survey of Mars For Opposition Years 1965-1995*. Association of Lunar and Planetary Observers (ALPO), Memphis, TN.
- Kahre MA, H. R. (2010). Mars CO₂ cycle: Effects of airborne dust and polar cap ice emissivity. *Icarus*.
- Kass DM, K. A. (2016). *Interannual similarity in the Martian atmosphere during the dust storm season*.
- Kass, D. M. (2020). *Mars Climate Sounder Observation of Mars' 2018 Global Dust Storm*.
- Kleinböhl, A. A. (2020). Diurnal variations of dust during the 2018 global dust storm observed by the Mars Climate Sounder. *JJournal of Geophysical Research: Planets*, 125(1). doi:10.1029/2019JE006115
- Leovy, C. B. (1979). Thermal tides and Martian dust storms: Direct evidence for coupling. *Journal of Geophysical Research: Solid Earth*, 84(B6), 2956-2968.

- Leovy, C. E. (1973). Mechanisms for Mars dust storms. *Journal of Atmospheric Sciences*, 30(5), 749-762. Retrieved from https://journals.ametsoc.org/view/journals/atsc/30/5/1520-0469_1973_030_0749_mfmds_2_0_co_2.xml
- Li B, Y. Z. (2021). Spatio-Temporal Analysis of Dust Storm Activity in Chryse Planitia Using MGS-MOC Observations from Mars Years 24–28. *Universe*.
- Martin, L. J. (1993). An analysis of the history of dust activity on Mars. *Journal of Geophysical Research*, 98(E2), 3221-3246.
- Martínez, G. M.-R. (2017). the modern near-surface Martian climate: a review of in-situ meteorological data from Viking to Curiosity. *Space Science Reviews*, 212(3-4), 1395-1444.
- Meteo Mars*. (2023). Retrieved from Meteo Mars: <https://meteomars.pamplonnetario.org/>
- MOLA. (2020). *Mars MGS MOLA DEM 463m v2*. GeoScience PDS Node.
- Morris, R. V. (2000). Mineralogy, composition, and alteration of Mars Pathfinder rocks and soils: Evidence from multispectral, elemental, and magnetic data on terrestrial analogue, SNC meteorite, and Pathfinder samples. *Journal of Geophysical Research: Planets*, 105(E1), 1757-1817.
- NASA. (2007). *MARCI Sees a Martian Dust Storm*. Retrieved from MARCI Sees a Martian Dust Storm: <https://mars.nasa.gov/resources/7888/marci-sees-a-martian-dust-storm/?site=msl>
- NASA. (2021). German Aerospace Center. Retrieved from Landing sites of Mars missions.
- NASA/JPL-Caltech. (2022, January 21). *Mars Report: Dust Storms on Mars*. Retrieved from [mars.nasa.gov](https://mars.nasa.gov/resources/26555/mars-report-dust-storms-on-mars/): <https://mars.nasa.gov/resources/26555/mars-report-dust-storms-on-mars/>
- Newman CE, D. M. (2020). *Toward More Realistic Simulation and Prediction of Dust Storms on Mars*.
- Observatory, E. (2022). *Dusty Differences Between Mars and Earth*. Retrieved from <https://earthobservatory.nasa.gov/images/149926/dusty-differences-between-mars-and-earth>
- PDS. (2023). Retrieved from The Cartography and Imaging Sciences Discipline Node: <https://pds-imaging.jpl.nasa.gov/>

- PDS. (n.d.). *The SPICE Concept*. Retrieved from JPL:
<https://naif.jpl.nasa.gov/naif/spiceconcept.html>
- QGIS. (2022). *Qgis2threejs Plugin Document*. Retrieved from QGIS:
<https://qgis2threejs.readthedocs.io/en/docs/>
- QGIS. (2023). Retrieved from QGIS: <https://www.qgis.org/en/site/>
- Renno NO, K. J. (2008). Electrical activity and dust lifting on Earth, Mars, and beyond. In K. J. Renno NO, *Planetary Atmospheric Electricity* (pp. 419-434).
- Ruff, S. W. (2004). Spectral evidence for zeolite in the dust on Mars. *Icarus*. Retrieved from
<https://www.sciencedirect.com/science/article/abs/pii/S0019103503003865#:~:text=Now%2C%20the%20EPF%2Dderived%20spectrum,zeolite%20in%20the%20martian%20regolith.>
- Sánchez-Lavega, A. A.-B.-G.-M.-E.-M. (2022). Cellular patterns and dry convection in textured dust storms at the edge of Mars North Polar Cap. *Icarus*.
- Savijärvi, H. (1994). Meteorology of the terrestrial planets. *Surveys in geophysics*.
- Shaheen F, S. N. (2022). Shadow method retrievals of the atmospheric optical depth above Gale crater on Mars using HRSC images. *Icarus*.
- Smith, D. E. (1999). The global topography of Mars and implications for surface evolution. *Science*, 284(5419), 1495-1503.
- Solarsena. (2021). *Solarsena*. Retrieved from Solar Azimuth Angle Calculator & Solar Panels: <https://solarsena.com/solar-azimuth-angle-calculator-solar-panels/>
- Strausberg, M. J. (2005). Observations of the initiation and evolution of the 2001 Mars global dust storm. *Journal of Geophysical Research: Planets*, 110(E2). Retrieved from Mars: the red planet.
- USGS. (2023). Retrieved from United States Geological Survey: <https://www.usgs.gov/>
- Wall, M. (2019, March 13). These Are the Last Photos NASA's Opportunity Rover Took on Mars. *space.com*. Retrieved from <https://www.space.com/mars-rover-opportunity-last-photographs.html>
- Wall, M. (2022). Rugged Mars has taken big bites out of the Curiosity rover's wheels (photos). *SPACE.COM*. Retrieved from <https://www.space.com/nasa-mars-rover-curiosity-wheel-damage-photos>
- Wang, H. a. (2015). The origin, evolution, and trajectory of large dust storms on Mars during Mars years 24–30 (1999–2011). *Icarus*, 251, 112-127.

- Webster, G. (2016, 6 10). NASA Mars Orbiters Reveal Seasonal Dust Storm Pattern. (T. Greicius, Ed.) *Jet Propulsion Laboratory*. Retrieved from <https://www.nasa.gov/feature/jpl/nasa-mars-orbiters-reveal-seasonal-dust-storm-pattern>
- Yiğit, E. (2023). Coupling and interactions across the Martian whole atmosphere system. *Nature Geoscience*, 1-10.
- Zubrin, R. (2008). *How to live on Mars: a trusty guidebook to surviving and thriving on the red planet*. Three Rivers Press.
- Zurek, R. W. (2007). An overview of the Mars Reconnaissance Orbiter (MRO) science mission. *Journal of Geophysical Research: Planets*. Retrieved from NASA: <https://mars.nasa.gov/mro/mission/overview/>

Appendix

The PYTHON Script of The Three-Dimensional Visualization of the Dust Storm Heights Distribution Result:

```
#Import Libraries
from mpl_toolkits import mplot3d
import numpy as np
import matplotlib.pyplot as plt

# Creating figure
ax = plt.axes(projection='3d')
fig = plt.figure(figsize=(15,15))
ax.scatter(., )
ax.scatter(., )
ax.scatter(., )

# Creating color map
my_cmap = plt.get_cmap('hot')

# Adding labels
ax.set_xlabel("")
ax.set_xlim(,)
ax.set_ylabel("")
ax.set_ylim(,)
ax.set_zlabel("")
ax.set_zlim(,)
ax.set_title("")

plt.show
```

The PYTHON Script of the Contour Map Represents the Heights of Dust Result:

```
#Import Libraries
import numpy as np
from scipy.interpolate import griddata
import matplotlib.pyplot as plt
from numpy.random import randn
from scipy import array, newaxis
from mpl_toolkits.axes_grid1.anchored_artists import AnchoredSizeBar
import matplotlib.font_manager as fm

#Adding Data
DATA = array([
    [ ,.],
    [ ,.],
    [ ,.],
])

x = DATA[:,0]
y = DATA[:,1]
z = DATA[:,2]

def plot_contour(x,y,z,resolution = 50,contour_method='linear'):
    resolution = str(resolution)+'j'
    X,Y = np.mgrid[min(x):max(x):complex(resolution), min(y):max(y):complex(resolution)]
    points = [[a,b] for a,b in zip(x,y)]
    Z = griddata(points, z, (X, Y), method=contour_method)
    return X,Y,Z

X,Y,Z = plot_contour(x,y,z,resolution = 50,contour_method='linear')
```

```
with plt.style.context("classic"):
    fig, ax = plt.subplots(figsize=(15,15))
    ax.scatter(x,y, color="black", linewidth=1, edgecolor="ivory", s=50)

# Adding labels
ax.set_xlabel("")
ax.set_xlim(,)
ax.set_ylabel("")
ax.set_ylim(,)
ax.set_title("")

plt.show()
```

Video of the 20 of May 2020 Dust storm result using QGIS:

[file:///C:/Users/user/OneDrive/Desktop/New%20folder%20\(2\)/index.html](file:///C:/Users/user/OneDrive/Desktop/New%20folder%20(2)/index.html)

Video of the 6 of June 2021 Dust storm result using QGIS:

<file:///C:/Users/user/OneDrive/Desktop/3dV/results/3d%20result/index.html>

UAEU

جامعة الإمارات العربية المتحدة
United Arab Emirates University



UAE UNIVERSITY MASTER THESIS NO. 2023: 27

This work generated a Three-Dimensional Visualization of Mars's local dust storms utilizing satellite images. The workflow began with the MeteoMARS tool identifying the local dust storm by viewing MARCI\MRO images and then using NASA PDS to download the raw images. After that, the Integrated Software for Imagers and Spectrometers processes the images and generates the files required for calculating the main features of a Mars dust storm. Then, the calculations of the dust height from the dust storm's shadow that projected in the image. Finally, the visualization was then created using PYTHON and QGIS software.

Meirah Alzeyoudi: received her Master of Space Science from the Department of physics, College of Science and her bachelor's in urban planning with a minor of Geographic information systems from the College of College of Humanities and Social Science, UAE University, United Arab Emirates.

www.uaeu.ac.ae

Online publication of thesis:
<https://scholarworks.uaeu.ac.ae/etds/>

UAEU عمادة المكتبات
Libraries Deanship

جامعة الإمارات العربية المتحدة
United Arab Emirates University



Digital Library Services Section - قسم الخدمات المكتبية الرقمية